scientific reports

Check for updates

OPEN

Microscopic damage evolution and physical–mechanical behavior of high-temperature red sandstone under varying heating and cooling durations

Mingze Qin[3], Yue Su[3], Xiaolan Wang[2]✉, Huawu Niu[2], Yifan Zhang[3], Dongxu Zhang[3] & Nan Qin[1,3]✉

The investigation into the cooling and heating duration is crucial for evaluating the aftermath of a fire incident. This study comprehensively analyzes the macroscopic and microscopic characteristics of red sandstone under high temperatures, heating, and cooling conditions, with temperatures ranging from 200 to 800 °C and heating/cooling durations ranging from 0.75 to 3 h and 0.5 to 54 h, respectively XRD and SEM techniques were employed to investigate mineral composition and microstructural changes. Multifactorial experiments explored the impact of these conditions on the rock's physical properties and assessed mechanical properties such as peak stress, peak strain, and elastic modulus. Data fitting with MATLAB was used to construct a damage constitutive model. The findings show that elevated temperatures and prolonged heating significantly alter the microstructure and composition of red sandstone, including pore formation, void development, and structural modifications. Heating induces cracking, voids, and chemical reactions, with extended exposure leading to changes in feldspar minerals (K/Ca/Na). Temperature-dependent physical properties exhibit mass loss and density decline. Mechanical properties are substantially affected, with peak stress decreasing from 40 MPa to 6.94 MPa, and variations in peak strain and elastic modulus. Thermal stress at specific temperatures notably enhances compressive strength. The newly established constitutive model has an error within 5% compared to actual experimental results.

Keywords Heating and cooling time, Microscopic damage, Multifactorial, Constitutive model

The development of tunnels, buildings, underground facilities, and mines constitutes an essential component in the progression of modern urbanization. These projects frequently present intricate engineering and technical obstacles, with safety precautions being particularly vital[1]. Fire safety incidents are a frequent occurrence globally. Using China as a case study, it has been observed that over 100,000 fires transpire annually, with the majority being urban fires. These fires resulted in more than 1,000 fatalities[2].What's worse, secondary collapse incidents, triggered by fires in tunnels, buildings, and underground facilities, are also reported intermittently. Therefore, evaluating the risk of collapse and predicting fire characteristics—such as combustion duration, cooling time, and the nature of the rock mass—hold significant engineering value. This is crucial for ensuring the safety of search and rescue personnel and minimizing potential secondary injuries. Furthermore, during the extraction of energy or mineral resources, the underground rock mass often retains a certain temperature. Determining the appropriate cooling time before mining is another critical challenge in such projects[3]. Consequently, it is imperative to investigate the properties of the rock mass under the influence of high temperatures, heating durations, and cooling time.

The evolution of physical and mechanical properties and their genetic mechanism under high temperatures is a key area of interest. Researchers have done a lot of research to reveal microstructural changes in rocks at high

[1]Liaoning Technical University Liaoning Key Laboratory of Mining Environment and Disaster Mechanics, Fuxin 123000, China. [2]Mount Taishan Vocational and Technical College, Taian 271000, China. [3]School of Mechanical and Electrical Engineering, Qingdao University of Science and Technology, Qingdao 266061, China. ✉email: 584500750@qq.com; qinnan_qust@126.com

temperatures, including mineral phase transitions, particle diffusion, and rearrangements. These microscopic changes have a significant impact on the physical properties (e.g., hardness, toughness, electrical conductivity) and chemical properties (e.g., acid resistance, redox activity) of the rock. On a microscopic scale, Gao et al. successfully delineated the high-temperature metamorphic history[4] by employing scanning electron microscope (SEM) images in conjunction with deep learning technology. Hu et al. investigated the micromorphological features of different rocks and combined the micromechanical properties to construct the temperature-dependent failure criterion[5]. AK Verma, MK Jha et al. Thermal conductivity was predicted by using scanning electron microscopy SEM to study internal microstructure changes within shale and combine P-wave velocity and porosity. It shows that the porosity of shale increases to 2.3 times its initial temperature.[6]. Li et al. used the acoustic emission (AE) monitoring technology to study the acoustic emission signal under uniaxial compression of yellow sandstone, and revealed the acoustic characteristics, crack types,and evolution of rock destruction process, to better explain the mechanism of the rock destruction[7]. Shen et al. used NMR resonance (NMR) technology to analyze the microstructural evolution of the samples and determined the microscopic damage evolution law at high temperatures by comprehensively analyzing mechanical parameters, T2 spectra, NMR imaging, X-ray diffraction pattern ,and porosity[8]. L.P et al. studied the influence of temperature on the physical and mechanical properties of rock, especially thermal damage on granite. The physical properties and thermal damage mechanism of granite at different temperatures were revealed by polarizing microscopy, ultrasonic detection, and XRD physical characterization[9].

In macroscopic mechanical analysis, Ding et al. examined the impact of temperature (200–800℃) and limiting pressure (20–40 MPa) on the mechanical attributes of sandstone. Their findings revealed that above 400℃, there was a significant increase in the peak stress of the rock, while simultaneously, the peak payload stress exhibited a marked decrease as the temperature escalated[10]. Xiao et al. performed cyclic loading and unloading tests on sandstone treated at varying temperatures (25–800℃) and developed an energy calculation equation[11] that takes into account both constraint pressure and seepage pressure. Yang et al. conducted a study to examine the impact of fracture angle and heat treatment temperature on the mechanical properties and deformation of rock. They performed a uniaxial compression test on granite samples with a single fracture, utilizing a strain gauge to measure the local strain around the existing fracture. The full strain field and local strain concentration were discussed, and the fracture mechanism of brittle granite was described[12]. Li et al. employed the fractal theory method in conjunction with the Grassberg-compu calculation (G-P) algorithm to elucidate the fracture mechanism of rock[13]. In earlier studies, Yavuz H examined the mechanical properties of limestone post-high temperature exposure, while Chen investigated the alterations in granite's mechanical properties under high temperatures using a uniaxial compression test. Their findings indicated that as temperature increased, both peak stress and elastic modulus decreased progressively, while peak strain increased consistently.[14,15]. Brotons investigated into the impact of temperature on the mechanical properties of carbonate rocks. The findings indicate that as the temperature escalates within the range of 105–600℃, there is a gradual decrease in the uniaxial compressive strength, elastic modulus, and Poisson's ratio by[16]. Wu examinated of the mechanical properties of sandstone under high temperatures ranging from 20–1200℃, providing a detailed analysis of the entire stress–strain process. The findings indicated that as the temperature increased, both the peak strength and Young's modulus progressively diminished. Conversely, the Poisson ratio typically demonstrated a pattern of initial increase, followed by a decrease, and then another increase[17]. J. Yu conducted a comprehensive study on the mechanical properties and permeability evolution of red sandstone[18].

The heating duration of rock, defined as the time during which it is subjected to heat in an experiment, serves as a crucial metric for studying the damage sustained by rock at a constant temperature. This process mirrors real-world scenarios such as the continuous combustion within residential structures, mines, tunnels, and the high-temperature environments encountered in underground energy extraction. Over the years, scholars have employed a range of experimental apparatus and methodologies to replicate the rock heating process under varying temperatures and pressures. Their findings suggest that the heating duration is influenced by factors such as rock composition, particle size, and heating rate.

Gu et al. utilized a servo-controlled compression device to examine the mechanical properties of sandstone, marble, and granite under real-time heating conditions. The study suggests that the mechanical behavior of rock subjected to real-time heating differs from its behavior under standard conditions. By controlling the duration of real-time heating, the accuracy of both theoretical and numerical analyses can be enhanced[19]. Hassani, F. et al. conducted a study on the impact of microwave radiation on the temperature profile and intensity reduction of various types of hard rock, including brown rock, granite, and basalts under different exposure times and microwave power levels. The study concluded that both tensile strength and uniaxial compressive strength decrease as exposure time and power level increase[20]. Tang et al.[21] conducted a study to examine the impact of varying temperatures (i. e., 20, 200, 300, 400, 500, and 600℃) and durations (i.e.,0.5, 1, 2, 3, 4, and 8 h). When lower treatment temperatures are found, the effect of high -temperature time on rock behavior is significantly not negligible. In addition to heating duration, the effect of heating cycle time on rock is still significant, Zhang et al. studied the effect of thermal cycle treatment on granite microfracture expansion and mechanical behavior and found that the degradation trend of granite UCS value and elastic modulus can be characterized by heating temperature and thermal cycle time for[22].

The study of rock cooling time was conducted to investigate the duration required for a rock to cool following thermal damage. This research enhances our understanding of the cooling process in high-temperature rocks within an engineering context. The practical application of this study is significant in engineering practice. For instance, the precise control of the post-heating rock cooling process in construction projects such as buildings, bridges, and mine-laying can enhance the stability and durability of the structures. In the field of mining engineering, comprehending the process of rock cooling can significantly contribute to the optimization of mining procedures. This understanding can lead to cost reductions and enhance overall efficiency. To achieve

this objective, researchers such as Kim, K et al. conducted a series of laboratory experiments to study the impacts of rapid thermal cooling on various rock samples, encompassing igneous, sedimentary, and metamorphic rocks. Initially, different types of thermal loading were applied: heating to 100, 200, and 300℃, followed by rapid cooling using a fan. The number of repeated thermal cooling cycles was controlled (10, 15, 20 times) to induce varying degrees of rock cracking[23]. Wang, H et al. employed the straight cracked Brazilian disc (CSTBD) sample to investigate the fracture performance of granite across a temperature range of 25℃ to 800℃, with varying water cooling times. The study aimed to ascertain the impact of water cooling duration on the engineering rock mass following exposure to different temperatures[24]. Yang, K et al. studied the safety and reliability effects of high-temperature processing and cooling time on the physical and mechanical properties of rocks. Found that the sample gradually changed from shear to split failure with increasing cooling time after 600℃ treatment[25]. Zhang, Z. introduces an enhanced temperature control scheme for mine compressed air, ice storage tanks, and the surrounding rock formations. The study reveals that during the pre-cooling phase, the temperature of the surrounding rock decreases exponentially over time. Furthermore, the temperature gradient diminishes as both the ventilation rate and ventilation temperature increase. However, the correlation with the initial temperature of the surrounding rock appears to be minimal[26].

In a study of cooling and heating time conditions, Mo et al. observed that heat-induced microcracks emerged during the heating phase and were detectable in real-time cooling and heating periods. Conversely, during cooling, they noted the closure of existing cracks and microcracks. The real-time measurements of the micromechanical properties of minerals might be correlated with the macroscopic mechanical behavior of rocks under fluctuating temperature conditions, attributable to these heat-induced microcracks[27].

Previous research indicates that the effects of higher temperatures on the microscopic, physical, and mechanical properties of rocks have been relatively underexplored. The field of high-temperature research, specifically concerning the heating time condition, requires further exploration. Notably, there is a lack of understanding regarding the microscopic changes that occur due to the influence of heating time. Furthermore, the impact of cooling duration on rock behavior warrants a thorough investigation, with the duration and temperature fluctuations serving as critical parameters. Microscopically, past research has predominantly concentrated on X-ray diffraction (XRD) analysis at varying temperatures. In this study, we extend the analysis to consider the influence of heating duration on diffraction intensity and the patterns of material alteration under different heating intervals. On a macroscopic scale, while scholars typically integrate heating and cooling processes for real-time analysis, in practical engineering contexts, such as disaster assessment, the analysis of rock mechanical behavior under the combined effects of high temperatures, heating duration, and cooling time is particularly crucial and thus holds significant research potential.

Materials and methods

Materials and sampling

In this study, Zigong City, Sichuan Province was used as the specimen material. By the machining accuracy requirements set forth by the International Society of Rock Mechanics (ISMR) and the National Institute of Rock Mechanics and Rock Engineers (Ulusay and Hudson 2007), core specimens were prepared in line with standard laboratory specifications for cylindrical samples, measuring 50 mm in diameter and 100 mm in height. Given that the core undergoes initial processing via an automatic rock corer, some degree of error is inherent. The origin of the rock and the specific rock sample are illustrated in Fig. 1. The height deviation of the specimen is maintained within ± 0.5 mm, and similarly, the diameter deviation is also constrained to a range of ± 0.5 mm. To counteract the potential influence of overdispersion among rock samples on the precision of test outcomes, a comprehensive sampling strategy was implemented adhering to the Chinese standard GB/T 50,266–2013. A total of over 150 samples were meticulously collected across a range of temperatures: 400 °C, 600 °C, 800 °C, and 1000 °C, which were denoted as categories B, A, S, and Q respectively. The samples were subjected to controlled heating durations of 0.75 h, 1.5 h, and 3 h. Following the heating process, the samples underwent cooling periods of 0.5 h, 6 h, 30 h, and 54 h. An extensive dataset was compiled from over 150 samples, from which a representative subset of 49 data points was strategically chosen, maintaining a ratio of 1:3 as indicated in reference[28]. For analysis, one specimen was designated as the benchmark, while the remaining 48 specimens were systematically allocated into four distinct groups, each encompassing 12 specimens. An outline of the preliminary physical parameters and the numbering criteria for these samples is provided in Table 1 below.

Test process

In this study, the specimen was subjected to treatment using an RPH-80 constant temperature and humidity box, an integrated intelligent muffle furnace, and a TAW-200 electronic material mechanical testing machine. The aim was to investigate the impact of temperature and time thresholds on the physical and mechanical properties of rock. Concurrently, the specimens, both pre and post-thermal damage, were analyzed from a microscopic perspective. The XRD diffractometer was employed to analyze the components of the rock sample, while the structure morphology was observed using SEM[29]. Given that sandstone possesses a complex microstructure and significant anisotropy, its mechanical properties and behavior are likely to change under conditions of high temperature and pressure. Therefore, through the analysis of physical properties, mechanical properties, and microscopic composition changes, and by conducting a quantitative analysis to determine the uniaxial compressive strength and certain load creep as the evaluation index, this study aims to explore the equivalent law of temperature-heating time-cooling time. The ultimate goal is to establish a rock damage model equation. The test procedure is illustrated in Fig. 1.

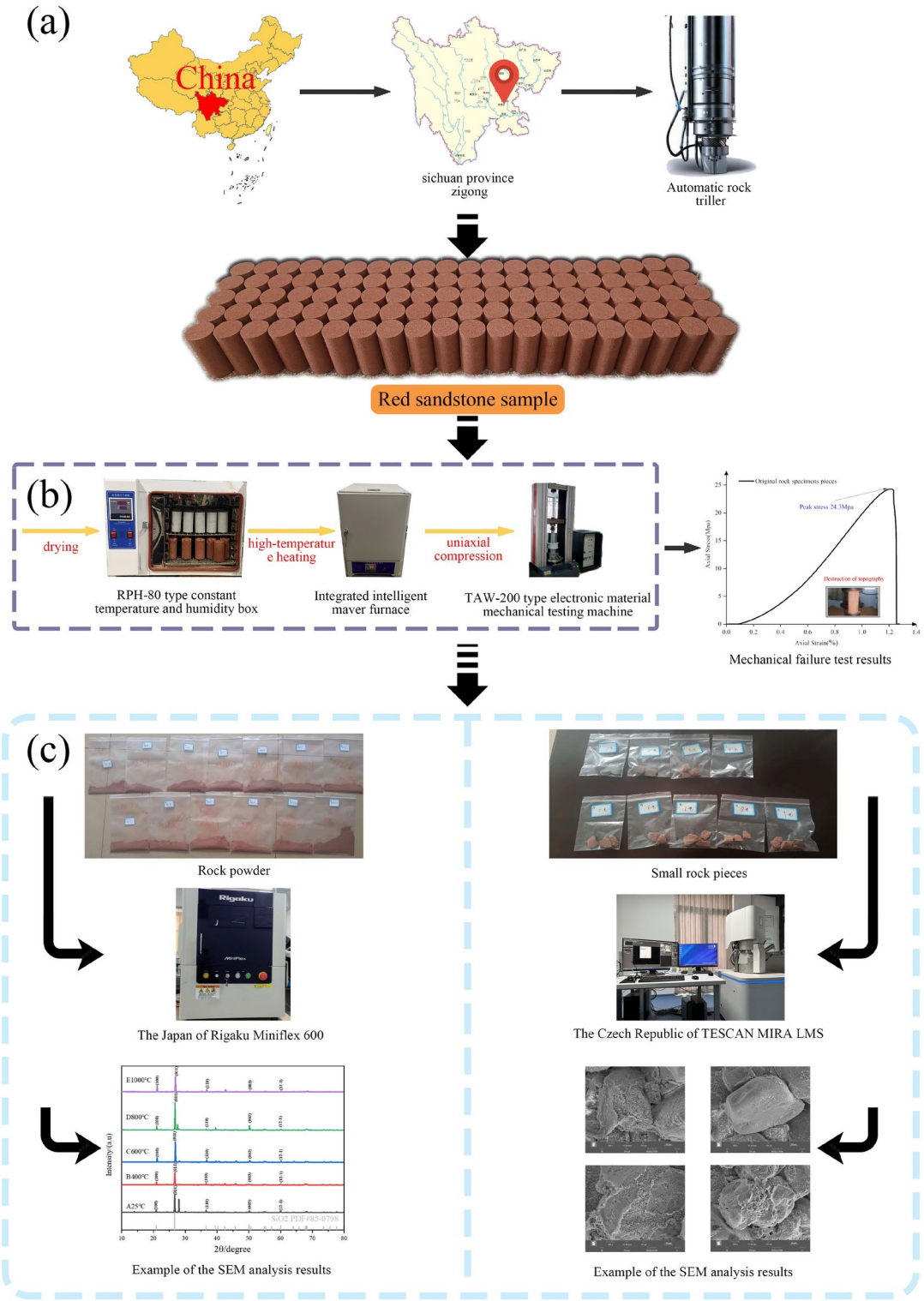

Fig. 1. Macro, micro-uniaxial destruction and creep test scheme of high-temperature red Sandrock.

Test structure and analysis

In this study, the physical parameters of 100 rock specimens were measured. Specimens with similar mass, volume, and density were chosen for heating at identical temperatures. The heating temperatures were set at 400, 600, 800, and 1000 ℃, while the heating durations were 0.75, 1.5, and 3 h. The cooling periods were 0.5, 6, 30, and 54 h. It is important to note that the term "heating temperature" refers to the process of elevating the specimen's temperature from 25 ℃ to the predetermined set temperature in the muffle furnace. The "heating time" denotes the duration for which the specimen is maintained at the set temperature, and the "cooling time" represents

400℃ number	600℃ number	800℃ number	1000℃ number
B0.75–0.5/B1	A0.75–0.5/A1	S0.75–0.5/S1	Q0.75–0.5/Q1
B0.75–6/B2	A0.75–6/A2	S0.75–6/S2	Q0.75–6/Q2
B0.75–30/B3	A0.75–30/A3	S0.75–30/S3	Q0.75–30/Q3
B0.75–54/B4	A0.75–54/A4	S0.75–54/S4	Q0.75–54/Q4
B1.5–0.5/B5	A1.5–0.5/A5	S1.5–0.5/S5	Q1.5–0.5/Q5
B1.5–6/B6	A1.5–6/A6	S1.5–6/S6	Q1.5–6/Q6
B1.5–30/B7	A1.5–30/A7	S1.5–30/S7	Q1.5–30/Q7
B1.5–54/B8	A1.5–54/A8	S1.5–54/S8	Q1.5–54/Q8
B3-0.5/B9	A3-0.5/A9	S3-0.5/S9	Q3-0.5/Q9
B3-6/B10	A3-6/A10	S3-6/S10	Q3-6/Q10
B3-30/B11	A3-30/A11	S3-30/S11	Q3-30/Q11
B3-54/B12	A3-54/A12	S3-54/S12	Q3-54/Q12

Table 1. Test piece processing number.

the natural cooling period before the uniaxial compression test, during which the specimen cools down to the ambient outdoor environment. The study examined the physical properties and uniaxial compression data of 48 rock specimens post-heat loss, as well as the uniaxial compression data of one undamaged specimen. Specimens suspected to have undergone microscopic composition changes were selected as the control group for X-ray diffraction (XRD) and scanning electron microscopy (SEM) testing[29]. The underlying mechanisms were analyzed by integrating both microscopic and macroscopic analyses.

Changes in microstructure and mineral composition

The microstructure and mineral composition of sandstone are significantly influenced by temperature. Prolonged cooling periods following high-temperature exposure often result in notable alterations to its physical and mechanical properties. Consequently, both temperature and heating duration should be taken into account when investigating the microscopic changes in sandstone. By integrating Scanning Electron Microscope (SEM) feature analysis with X-ray Diffraction (XRD) technology, we can comprehensively examine the evolution of sandstone's microstructure and mineral composition under varying heating durations and temperatures. Figure 2 provides a visual representation of the microscopic characteristics of high-temperature red sandstone.

Utilizing Scanning Electron Microscopy (SEM) and X-ray Diffraction (XRD) analysis, it was observed that the specimens at normal temperature exhibited a pronounced massive and honeycomb structure. Numerous initial cracks were evident on the surface of the red sandstone, primarily resulting from physical damage rather than chemical alterations, though the connections remained relatively secure. The XRD analysis revealed that the primary component of the sandstone is silica, with the presence of potassium feldspar, sodium feldspar, and calcium feldspar minerals also detected.

In the specimen heated to 400℃, micro-cracks are observable, manifesting on the uniformly fired surface. The concurrent presence of minute pores and adhesion among distinct structures suggests a chemical reaction has taken place. XRD analysis reveals that despite the temperature increase to 400℃, silica remains the primary component. Additionally, potassium, sodium, and calcium feldspar are present, though calcium feldspar shows signs of dissipation. With extended heating durations, the emergence of aluminum silicate can be attributed to the partial decomposition of feldspar, resulting in its ionic state and subsequent formation of aluminum silicate.

In the experiment conducted at 600℃, a significant number of pores emerged in the honeycomb structure post-sintering. This process led to a reduction in parts of the honeycomb structure and a notable increase in the dissolved adhesion phenomenon, resulting in numerous closely interconnected components. Additionally, a large crystalline structure, indicative of burning, was observed. Concurrently, minor cracks parallel to the crystal were detected. The intensity of the chemical reaction escalated. XRD analysis showed that in addition to the original main component of silica, calcium feldspar decomposed and disappeared, the components of potassium feldspar and sodium feldspar still existed, but as the temperature increased, the two feldspar components began to dissipate. At the longest heating time, the calcium silicate was produced, and the aluminum silicate composition became more obvious.

In the specimen subjected to 800℃, significant crystal cracks and extensive structural fractures are evident. Part of the internal ladder structure becomes apparent, with a pronounced bonding effect that virtually eliminates any separation within the structure, thereby enhancing its integrity. At this temperature, the presence of potassium feldspar and calcium feldspar in the sandstone is negligible. The primary constituents are silica, silicate, and sodium feldspar. As the heating duration increases, sodium feldspar progressively diminishes, suggesting an intensification of the reaction.

In the specimen heated to 1000℃, significant dissolution effects and property alterations were observed. The structure began to transition towards a liquid solidification state, with the honeycomb structure evolving into a flocculent form and large cracks appearing. Some structures exhibited signs of solidification separation, potentially due to varying solidification times post-liquid phase. Concurrently, numerous solidified crystals emerged, enveloping the entire specimen. Upon reaching 1000℃, the feldspar composition in the sandstone essentially dissipated. After three hours of heating, the silicate composition became more pronounced, suggesting that internal reactions were still ongoing.

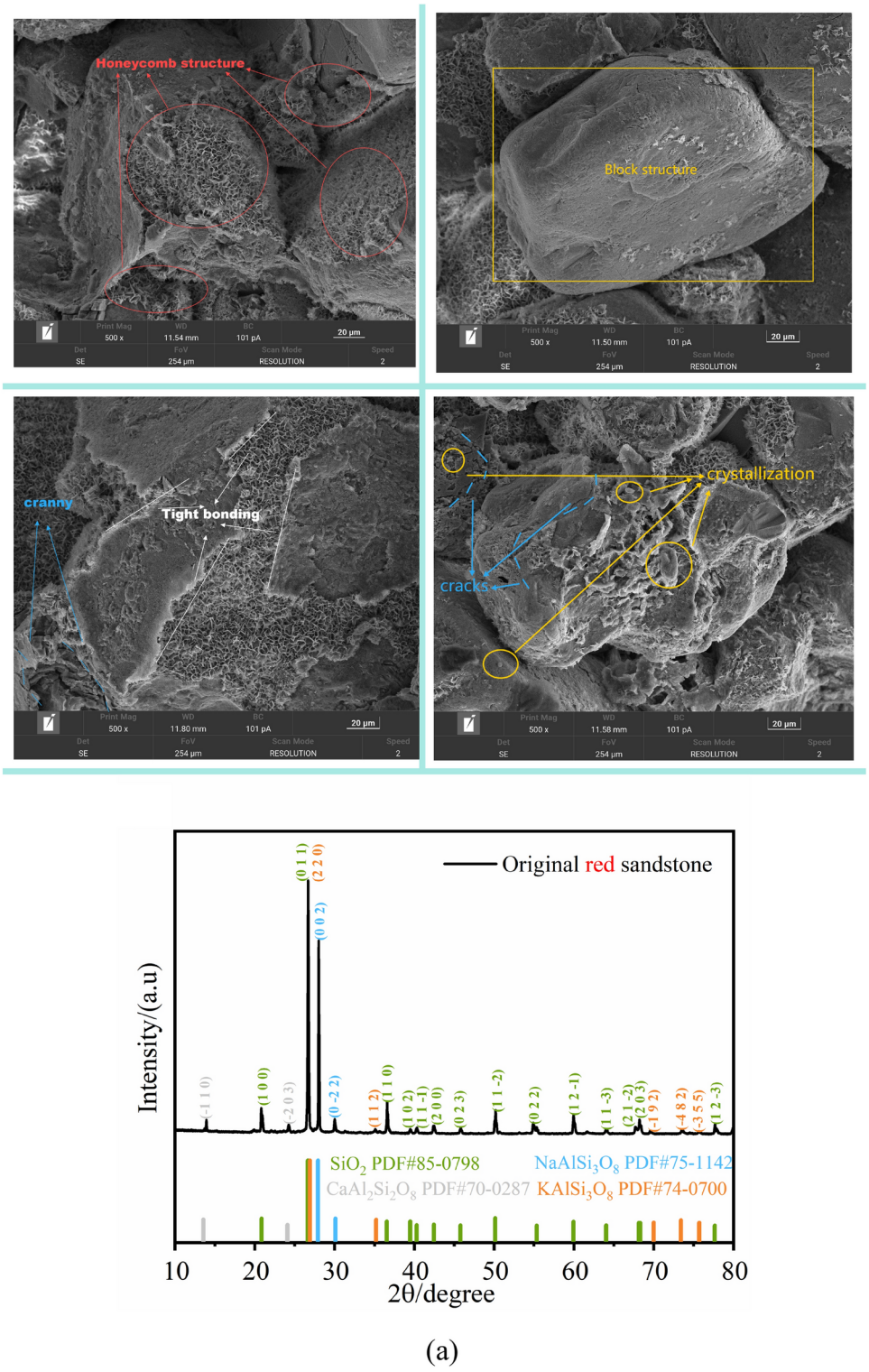

Fig. 2. Analysis of the microscopic characteristics of the high-temperature red sandstone.

Changes in physical characteristics

The process of thermal damage in rock often involves both physical and chemical reactions. These reactions directly result in significant alterations to the rock's mass, volume, density, and other physical properties. Wu, X et al. systematically reviewed the progression and development of deformation and destruction in hot rock masses. They introduced alterations in rock physical properties following exposure to high temperatures and real-time high- temperature conditions, thereby confirming the impact of thermal damage on these properties[30]. Zhang, Y., et al. investigated the deformation and destructive behavior of reservoir rocks in deep geothermal

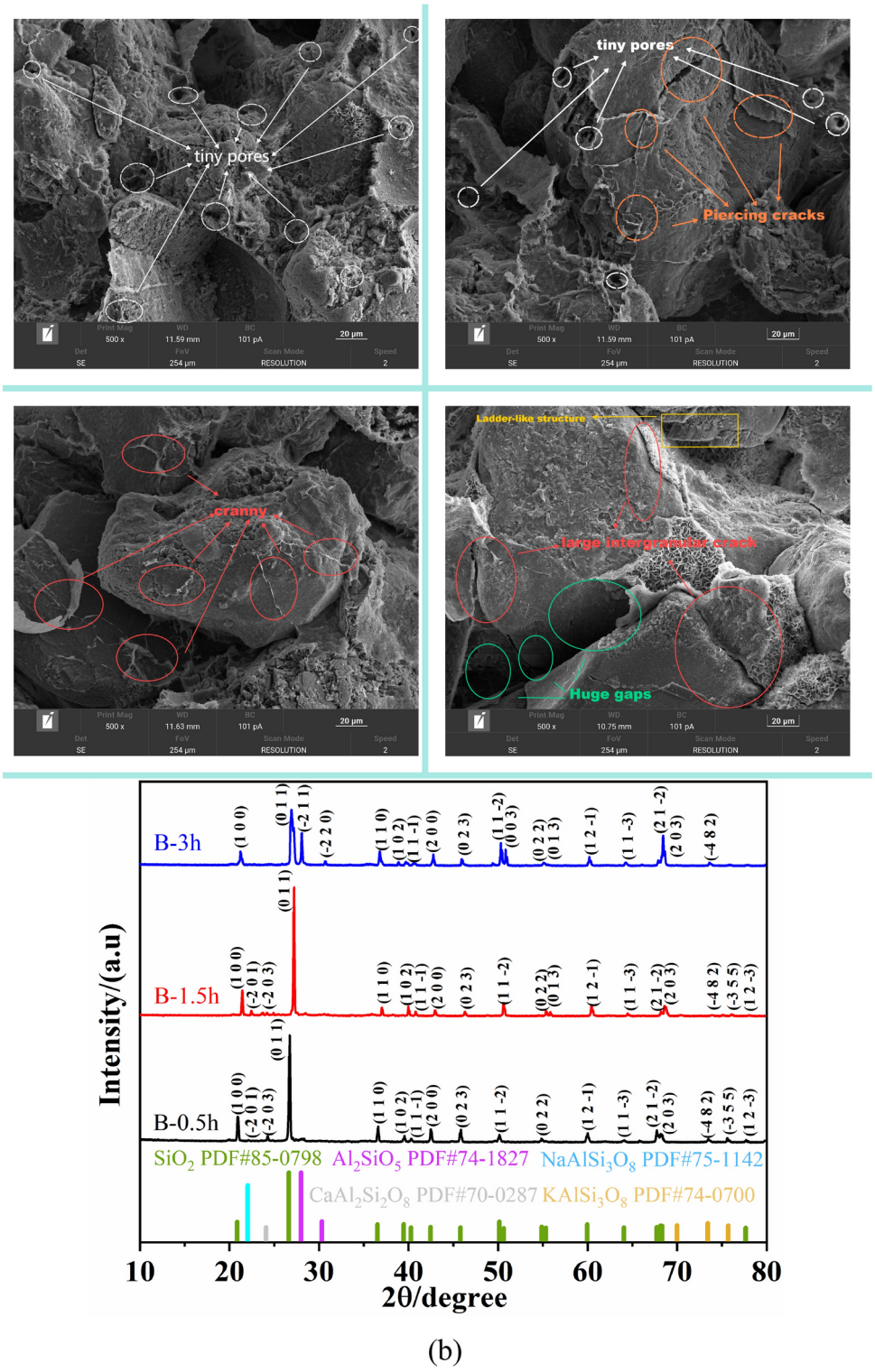

Figure 2. (continued)

engineering, which introduces cooling damage. This research contributes to the development of a new thermodynamic model, thereby providing a theoretical basis for the expression of rock physical properties[31]. In the context of damage parameter measurement, 48 specimens subjected to high-temperature testing were evaluated. The assessment involved calculating the mass damage amount, volume damage amount, density damage rate, mass damage rate, and density damage rate using the appropriate formulas. The primary variables influencing damage in this study were high temperature, cooling duration, and heating duration. To discern the impact of each factor more distinctly, a control variable approach was employed.

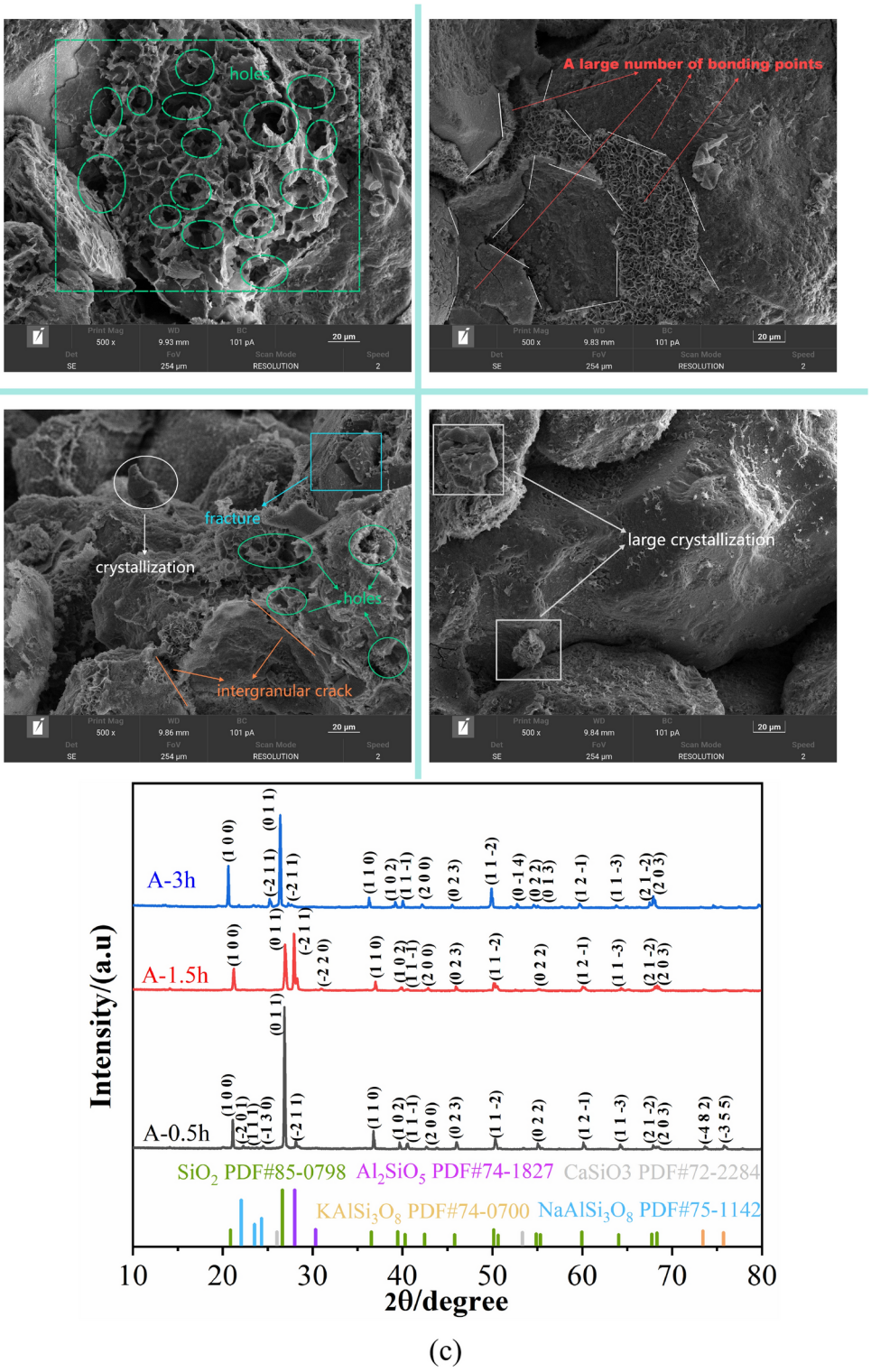

Figure 2. (continued)

To determine the physical properties under the influence of heating time and temperature, under the premise of not considering the influence of cooling time, according to the three heating times of four different temperatures, can be divided into 12 sets of data, the values of four different cooling time in each group of the data the 12 data points in Table 2, to consider the different temperature and heating time, organize the relevant data, and draw images as shown in Fig. 3.

When the cooling duration is disregarded, each heating time curve distinctly illustrates an increase in sandstone expansion, mass damage, and density damage between 400 to 800 ℃, with stability observed from

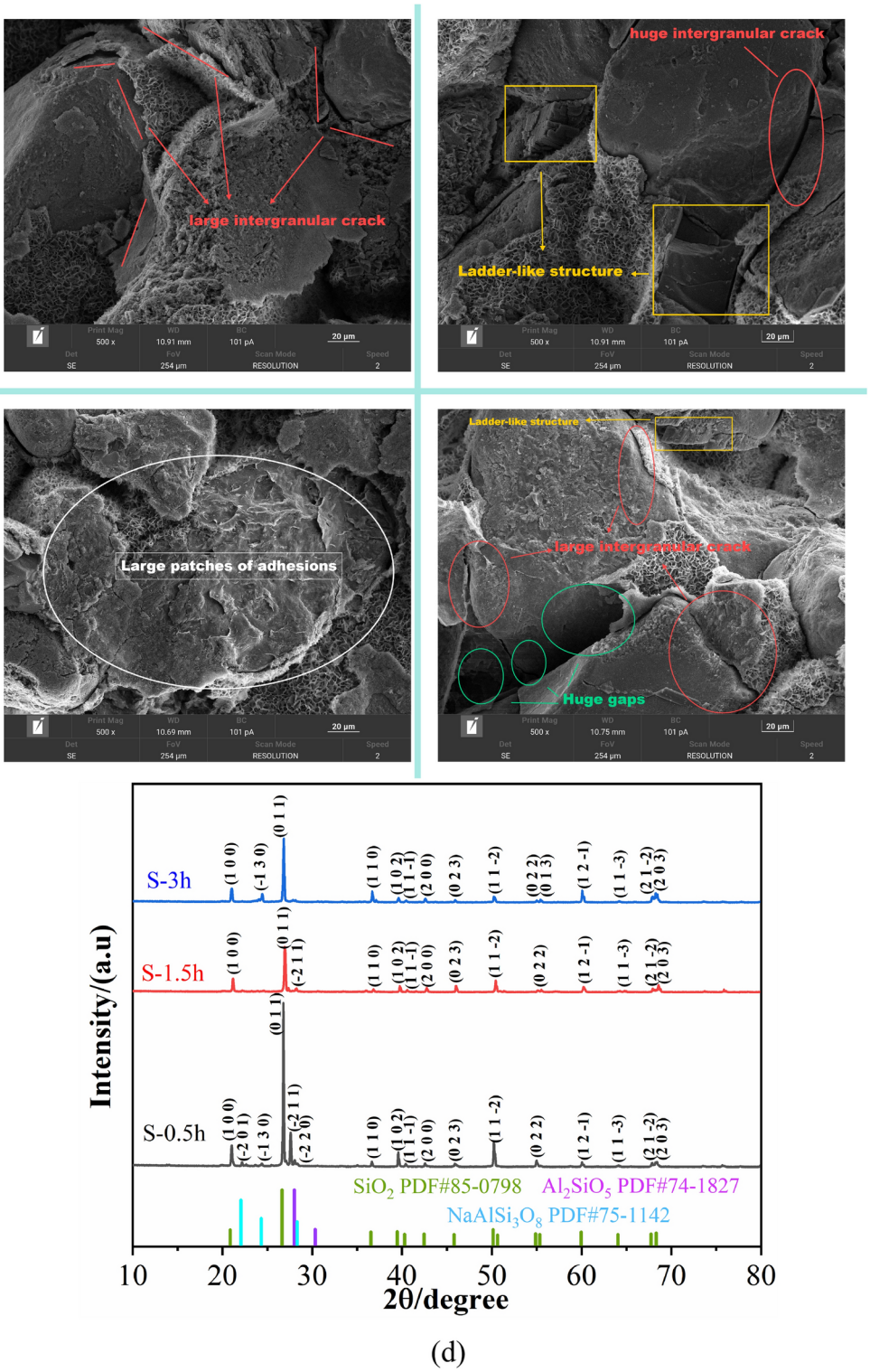

Figure 2. (continued)

800 to 1000 ℃. Furthermore, at a consistent heating temperature, it is evident that the magnitude of damage and the rate of loss for these three physical properties are significantly greater at 3 h compared to 0.75 h. In the process from 0.75 h to 3 h, the height of the numerical points increases with time.

To determine the physical properties under the influence of cooling time and temperature, all 48 specimens can be divided into 16 sets of data according to four cooling times at four different temperatures. The data values of three different heating times are averaged, and the 16 data points in Table 3 below are used to represent the

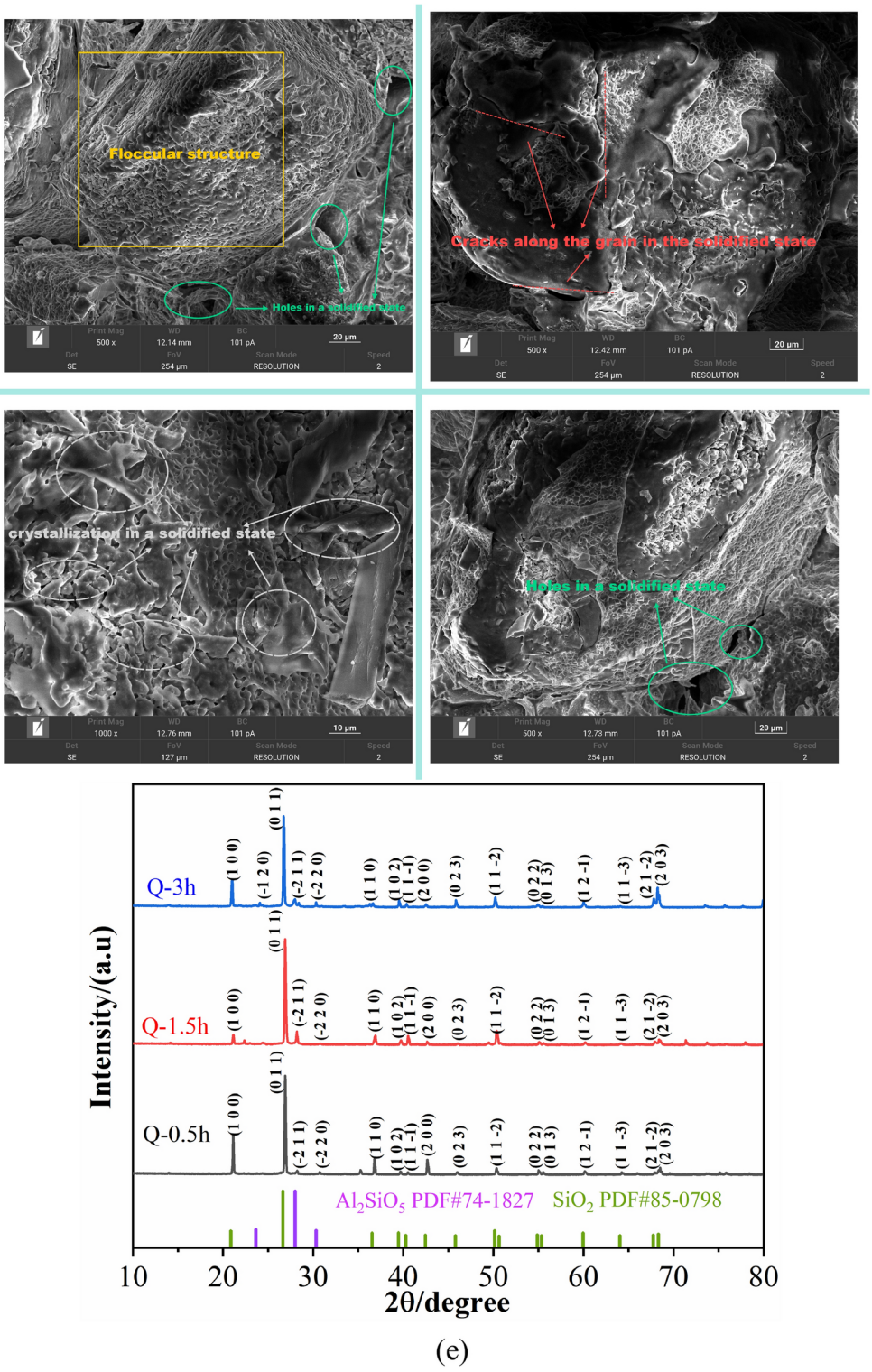

Figure 2. (continued)

data points under different temperatures and cooling times, organize the relevant data, and draw the image as shown in Fig. 4.

Regardless of the heating duration, when a specimen is heated at low temperatures (400–600℃), there is a noticeable decrease in both the damage rate and quantity of the sandstone mass. However, the volume expansion rate and quantity, as well as the density damage rate and quantity, exhibit a significant upward trend as the cooling time increases. When the specimen is subjected to high temperatures (800–1000℃), the effects become

	Number	Mass damage	Volume expansion	Density damage	Quality injury rate	Volume expansion rate	Density damage rate
temperature		$\Delta m = \frac{m_a - m_b}{m_a} \times 100\%$	$\Delta V = \frac{V_a - V_b}{V_a} \times 100\%$	$\Delta \rho = \frac{\rho_a - \rho_b}{\rho_a} \times 100\%$	$\frac{\Delta m}{\mathrm{m}}$	$\frac{\Delta V}{V}$	$\frac{\Delta \rho}{\rho}$
400℃	B0.75	-0.675	721.3530677	-1.13375E-05	-0.001721609	0.003801724	-0.005501295
	B1.5	-0.8	852.547716	-1.32644E-05	-0.002024123	0.004445784	-0.006439097
	B3	-0.975	1314.097945	-1.90691E-05	-0.002465335	0.006862143	-0.009262106
600℃	A0.75	-1.2	1317.36904	-2.03059E-05	-0.003066424	0.006900524	-0.009897222
	A1.5	-2.325	2651.005573	-3.97424E-05	-0.005884322	0.013762283	-0.019377543
	A3	-2.8	3630.087224	-5.25051E-05	-0.007134878	0.018972432	-0.025619512
800℃	S0.75	-4.35	4993.228457	-7.44325E-05	-0.011097046	0.026134737	-0.036272797
	S1.5	-4.7	6712.608871	-9.34922E-05	-0.011899633	0.035042402	-0.045350032
	S3	-4.8	6770.061723	-9.51059E-05	-0.012233776	0.035565994	-0.046154028
1000℃	Q0.75	-3.8	7794.923306	-0.000100004	-0.009675058	0.04087603	-0.048551831
	Q1.5	-4.175	8282.026853	-0.000106358	-0.010456157	0.043471498	-0.051673928
	Q3	-4.625	8458.99133	-0.000110123	-0.011773199	0.044215686	-0.053610991

Table 2. Variation of sandstone physical parameters under heating time–temperature influence.

more pronounced with longer cooling times. Specifically, the impacts observed during cooling periods of 54 h and 30 h are significantly greater than those seen during shorter cooling periods of 6 h and 0.5 h.

In this figure, it is evident that irrespective of the cooling duration, the temperature rises during the heating phase from 400 to 800℃. Furthermore, at 1000℃, the rate of volume expansion and the quantity continue to follow their original trends.

Uniaxial failure results of red sandstone

In this study, a TAW-200 mechanical compression tester was employed to establish a loading rate of 0.2 mm/min. The stress–strain curve was derived from the uniaxial compression test conducted on specimens under varying high temperatures, heating durations, and cooling times. Additionally, the morphological characteristics of the specimens at different temperatures were systematically arranged, as illustrated in Fig. 5.

Figure 5 clearly illustrates the trend of the curve as it relates to increasing temperature. Each figure visualizes the impact of both temperature and heating duration on the rock by tracking changes in the specimen from 0.5 h to 54 h under specific conditions of heating time and temperature. Under these conditions, it is observed that as the cooling time increases, the dispersion of the rock becomes more pronounced, its integrity becomes increasingly fragile, and its destructiveness intensifies. Furthermore, a lateral comparison at different temperatures reveals that higher temperatures result in more severe damage to the rock's morphology. When the temperature conditions are held constant, the heating time plays a significant role.

To conduct a more comprehensive study, it is crucial to examine the impact of cooling time, heating time, and temperature on the mechanical properties of rock specimens. This can be achieved by calculating the peak stress, peak strain, and elastic modulus of each specimen, thereby exploring the changes that occur due to these factors. To facilitate the observation of the corresponding independent variables, the heating time remains constant as depicted in Fig. 6, while the cooling time is kept consistent as shown in Fig. 7. This approach allows for an exploration of the influence of the remaining two factors on the mechanical properties of the specimen.

As illustrated in Fig. 7, the heating time remains constant, with every four points delineating the pattern of cooling time variation. Generally, both the peak stress and the elastic modulus exhibit a decreasing trend as the cooling time increases. However, the peak strain remains unaffected by changes in the cooling time. Furthermore, as the temperature rises, there is an overall decrease in the elastic modulus and peak stress, while the peak strain demonstrates an overall increase.

As illustrated in Fig. 7, the cooling time remains constant, with every three points denoting the trend of heating time variation. Overall, both the peak stress and the elastic modulus exhibit a decreasing trend as the cooling time increases. The peak strain escalates with the heating time at low temperatures and reaches a steady state at high temperatures, which could be attributed to changes in its properties. Furthermore, as the temperature rises, the elastic modulus and peak stress demonstrate a downward trajectory, while the peak strain displays an upward trend, remaining predominantly stable.

Discussion

Reasons for changes in microstructure and mineral composition

Utilizing a scanning electron microscope (SEM), we identified the presence of natural defects within the rock, primarily attributed to the water and gas trapped inside. In their natural state, these defects are relatively isolated; however, under external influences such as compression and grinding, they progressively interconnect, establishing a degree of continuity. Furthermore, X-ray diffraction (XRD) analysis conducted on rock samples at room temperature revealed that the primary components comprise silica (SiO_2), potassium feldspar ($KAlSi_3O_8$), sodium feldspar ($NaAlSi_3O_8$), and calcium feldspar ($CaAl_2Si_2O_8$). These findings align with the composition of natural minerals, thereby further substantiating the authenticity of the samples.

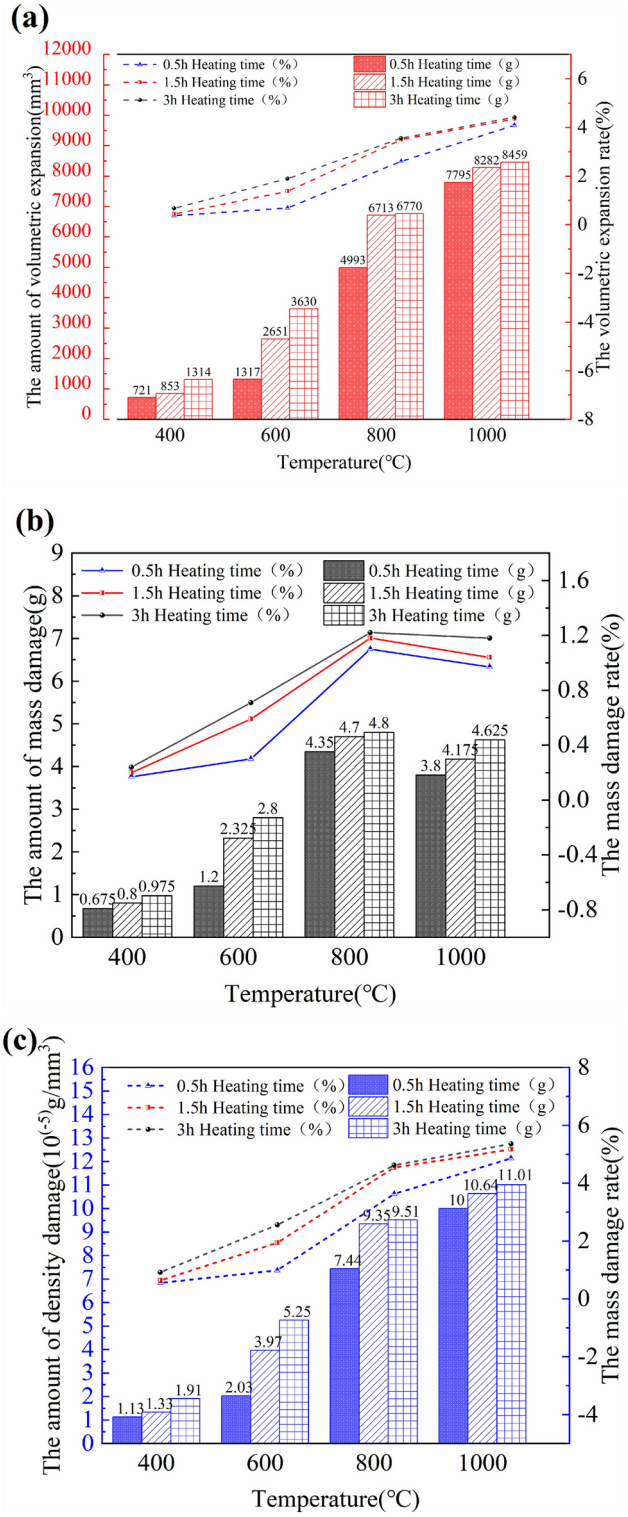

Fig. 3. Change of physical properties of red sandstone with temperature and heating time.

Upon increasing the temperature to 400 ℃, microscopic and perforating cracks emerged in the rock samples, primarily due to thermal damage. When the heating duration was extended to 3 h, an adhesion effect became apparent, suggesting that not only did the temperature influence microstructural changes, but the duration of heating also played a significant role. At 400 ℃, the newly formed aluminum silicate (Al_2SiO_5) was primarily produced by the decomposition of certain feldspar at elevated temperatures. After 3 h of heating, the calcium feldspar ($CaAl_2Si_2O_8$) completely vanished, indicating that the decomposition of calcium feldspar ($CaAl_2Si_2O_8$) into aluminum silicate (Al_2SiO_5) indeed occurred during the process.

	number	Mass damage	Volume expansion	Density damage	Quality injury rate	Volume expansion rate	Density damage rate
temperature		$\Delta m = \frac{m_a - m_b}{m_a} \times 100\%$	$\Delta V = \frac{V_a - V_b}{V_a} \times 100\%$	$\Delta \rho = \frac{\rho_a - \rho_b}{\rho_a} \times 100\%$	$\frac{\Delta m}{\mathrm{m}}$	$\frac{\Delta V}{V}$	$\frac{\Delta \rho}{\rho}$
400℃	B-0.5	-1.5	425.8572567	-1.23646E-05	-0.003794231	0.002214188	-0.005993491
	B-6	-0.966666667	785.2591662	-1.34608E-05	-0.002455968	0.004111837	-0.006538411
	B-30	-0.5	1249.004077	-1.59066E-05	-0.001264263	0.006506941	-0.007718305
	B-54	-0.3	1390.544472	-1.64962E-05	-0.00076696	0.007313235	-0.008019791
600℃	A-0.5	-2.8	1951.001716	-3.50405E-05	-0.007099852	0.010159177	-0.0170566
	A-6	-2.133333333	2464.958282	-3.71784E-05	-0.00544835	0.01292469	-0.018105887
	A-30	-2.066666667	2617.414263	-3.80362E-05	-0.005250417	0.013614204	-0.018580014
	A-54	-1.433333333	3097.908189	-3.98161E-05	-0.003648879	0.016148914	-0.019449869
800℃	S-0.5	-4.1	5743.836198	-8.06723E-05	-0.010458574	0.030063031	-0.039314826
	S-6	-4.4	5880.849388	-8.37884E-05	-0.011257509	0.030848032	-0.040835822
	S-30	-4.866666667	6290.44301	-9.03978E-05	-0.012357372	0.032937186	-0.043836221
	S-54	-5.1	6719.403473	-9.58489E-05	-0.012900485	0.035123851	-0.046382273
1000℃	Q-0.5	-3.833333333	7419.333867	-9.59017E-05	-0.009733982	0.038731007	-0.046649293
	Q-6	-3.9	7988.006481	-0.000102432	-0.009915975	0.041860281	-0.049694977
	Q-30	-4.366666667	8568.93088	-0.000110733	-0.011142871	0.045043496	-0.053763208
	Q-54	-4.6	8738.317424	-0.000112914	-0.01174639	0.045782835	-0.055008189

Table 3. Changes of sandstone physical parameters under cooling time–temperature.

Upon reaching a temperature of 600 ℃, a portion of the material undergoes decomposition within the sandstone, resulting in the formation of cavities and an enhancement of interconnectivity between these cavities as the duration of heating extends. X-ray diffraction (XRD) analysis revealed that calcium feldspar was entirely consumed after a mere 0.5 h of heating, whereas calcium silicate emerged upon heating for 3 h. This observation suggests that calcium feldspar ($CaAl_2Si_2O_8$) transformed $CaSiO_3$, subsequently releasing Ca^{2+} ions. Concurrently, the decomposition of sodium feldspar ($NaAlSi_3O_8$) might also contribute to the generation of aluminum silicate (Al_2SiO_5).

Upon reaching a temperature of 800 ℃, the rock structure exhibits notable changes including cracks, fissures, and evident adhesion. These alterations are directly associated with the prevailing high-temperature conditions, and their intensity amplifies as the duration of heating extends. XRD analysis further reveals that aside from silica (SiO_2), the diffraction patterns of silicate (Al_2SiO_5), sodium feldspar ($NaAlSi_3O_8$), and potassium feldspar ($CaAl_2Si_2O_8$) diminish in clarity. Notably, the presence of potassium feldspar vanishes entirely, suggesting a profound decomposition of the feldspar structure.

Upon reaching a temperature of 1000 ℃, molten liquid emerges within the rock sample, leading to a coagulation separation phenomenon in the structure due to varying solidification times post-liquid generation. Other structural features, such as holes, cracking, and flocculent structures, primarily arise from excessively high temperatures. At this juncture, the influence of heating duration is minimal, essentially achieved within 0.5 h of heating. XRD analysis indicates that all factors are affected by both high temperature and heating duration. Concurrently, the potential for aluminum silicate decomposition into silica (SiO_2) persists across different temperatures. The primary chemical reaction processes are detailed as follows:℃

$$CaAl_2Si_2O_8 \xrightarrow[\Delta]{400} 400Ca^{2+} + Al_2SiO_5 + CaSiO_3 \tag{1}$$

$$NaAlSi_3O_8/KAlSi_3O_8 \xrightarrow[1.5h\Delta]{600} Na^+/K^+ + Al_2SiO_5 \tag{2}$$

$$NaAlSi_3O_8 \xrightarrow[1.5h\Delta]{600} Na^+ + Al_2SiO_5 \tag{3}$$

$$CaAl_2Si_2O_8 \xrightarrow[\Delta]{800} Ca^{2+} + Al_2SiO_5 + CaSiO_3 \tag{4}$$

$$KAlSi_3O_8/NaAlSi_3O_8/CaAl_2Si_2O_8 \xrightarrow[\Delta]{800} K^+/Na^+/Ca^{2+} + NaAlSi_3O_8 + Al_2SiO_5 \tag{5}$$

$$KAlSi_3O_8/NaAlSi_3O_8/CaAl_2Si_2O_8 \xrightarrow[\Delta]{1000} K^+/Na^+/Ca^{2+} + Al_2SiO_5 \tag{6}$$

$$Al_2SiO_5 \xrightarrow[0.5-3h\Delta]{400-1000} Al^{3+} + SiO_2 \tag{7}$$

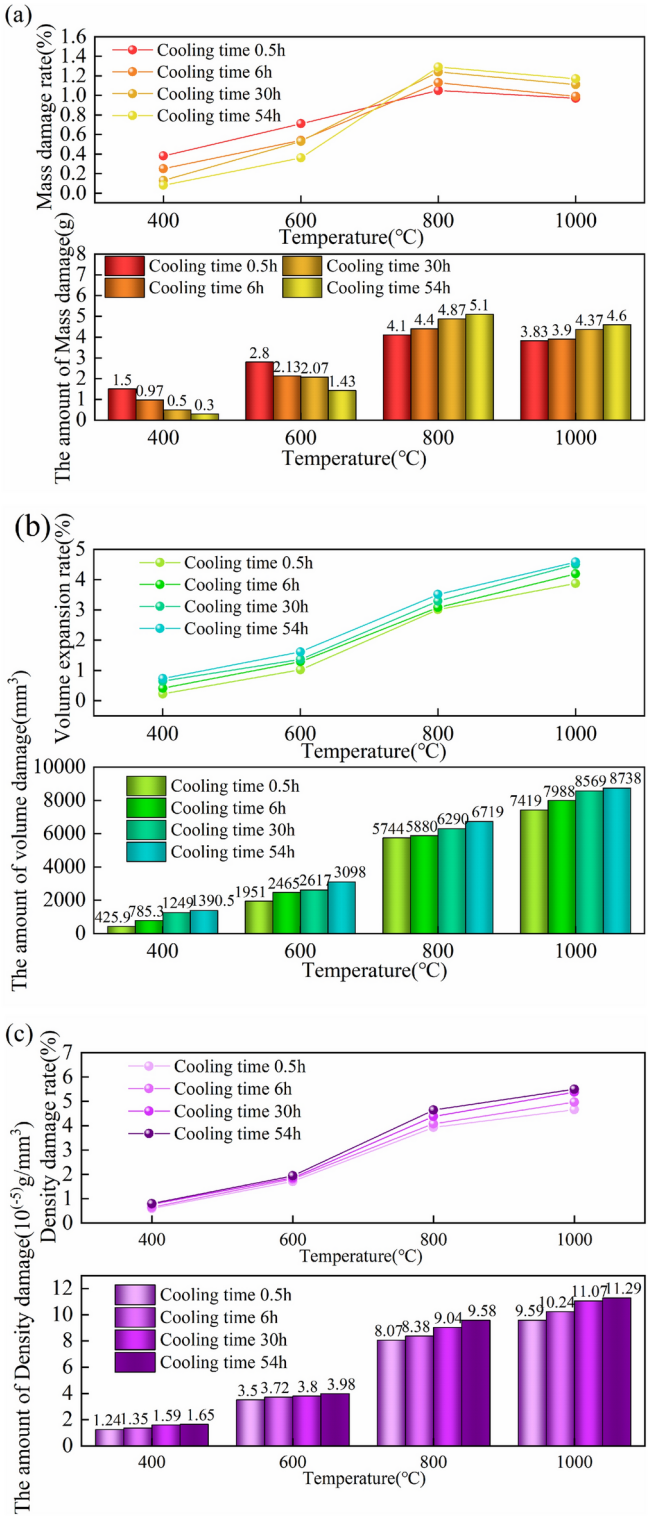

Fig. 4. Change of physical properties of red sandstone with temperature and cooling time.

Discussion of physical properties and mechanical properties of sandstone

Previous research has demonstrated that cooling duration, heating duration, and temperature exert significant influences on both the physical and mechanical properties of materials.

In terms of physical properties, microscopic analysis reveals that the evaporation of water within the specimen, the ionization of certain chemicals, and the extensive formation of pores during heating are the primary factors contributing to mass reduction. As the temperature rises, the degree of reaction among the reactants increases, leading to greater mass loss and a faster rate of mass loss. Under identical temperature conditions, prolonging

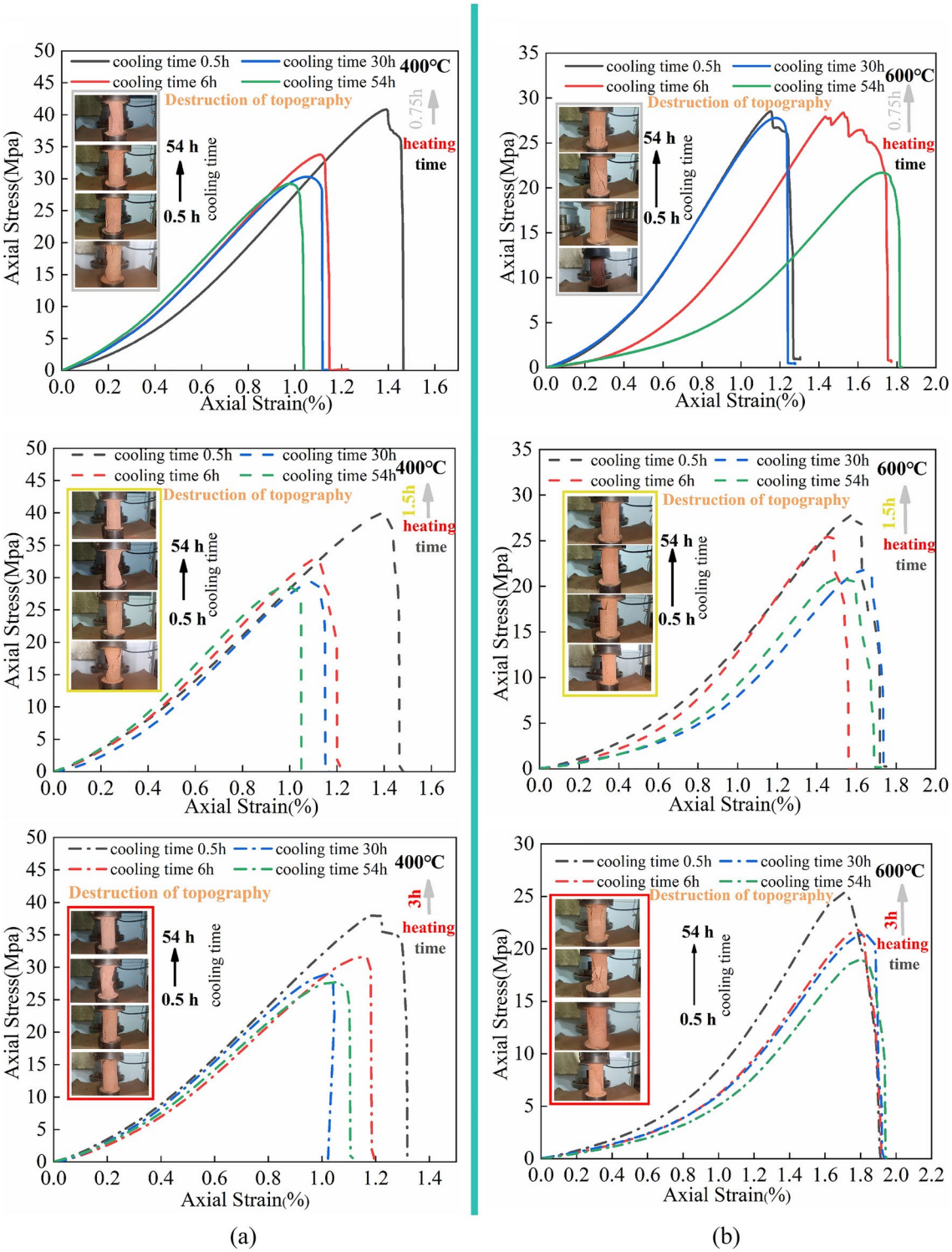

Fig. 5. Stress–strain and uniaxial damage morphology diagram of red sandstone.

the heating duration also results in increased mass loss, as some substances undergo chemical decomposition at high temperatures.

The expansion of the sandstone is characterized by an increase in volume, which is attributed to the growth of pores and the reaction of internal materials. This phenomenon is evident in both computational outcomes and microscopic examinations. Furthermore, elevated temperatures and prolonged heating durations typically result in a higher rate of volumetric expansion. This is because high temperatures and extended heating periods enhance the development of pores, cavities, and cracks within the sandstone. Regarding density variations, as the mass diminishes and the volume expands with increasing temperature and heating duration, the density

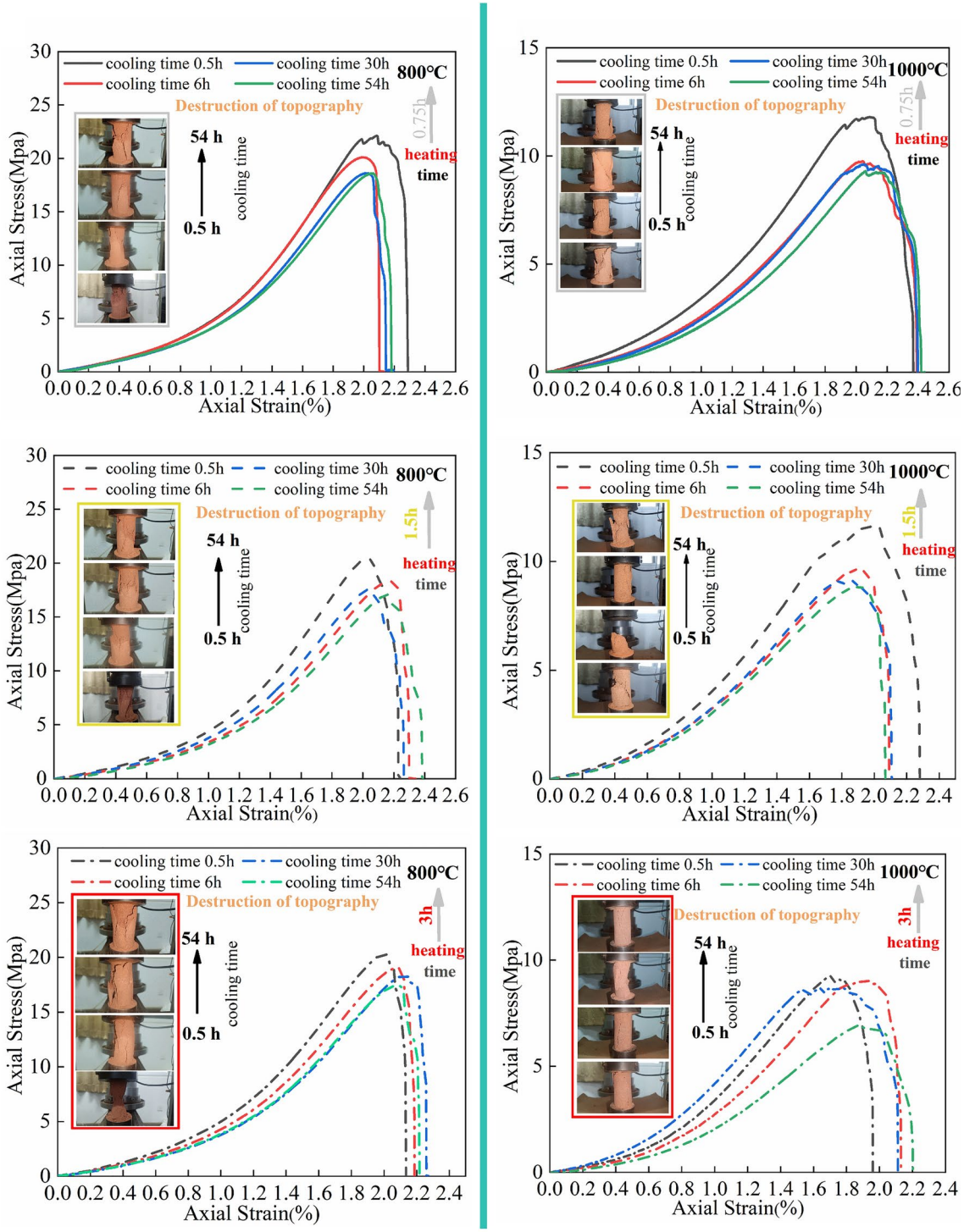

Figure 5. (continued)

subsequently decreases, as dictated by the density calculation formula. Additionally, the cooling period also influences the physical properties of the sandstone.

Upon exposure to high temperatures, sandstone is extracted from the Maver furnace and, over time, undergoes weathering, leading to surface powdering. Prolonged air exposure causes the sandstone to absorb moisture, resulting in a looser internal structure and further enlargement of pores. This, in turn, leads to volume expansion, mass reduction, and a subsequent decrease in density. Beyond the duration of cooling and heating, temperature fluctuations are the primary factors influencing the physical properties of sandstone. The trend in these properties with temperature is consistent with the aforementioned observations. However, when

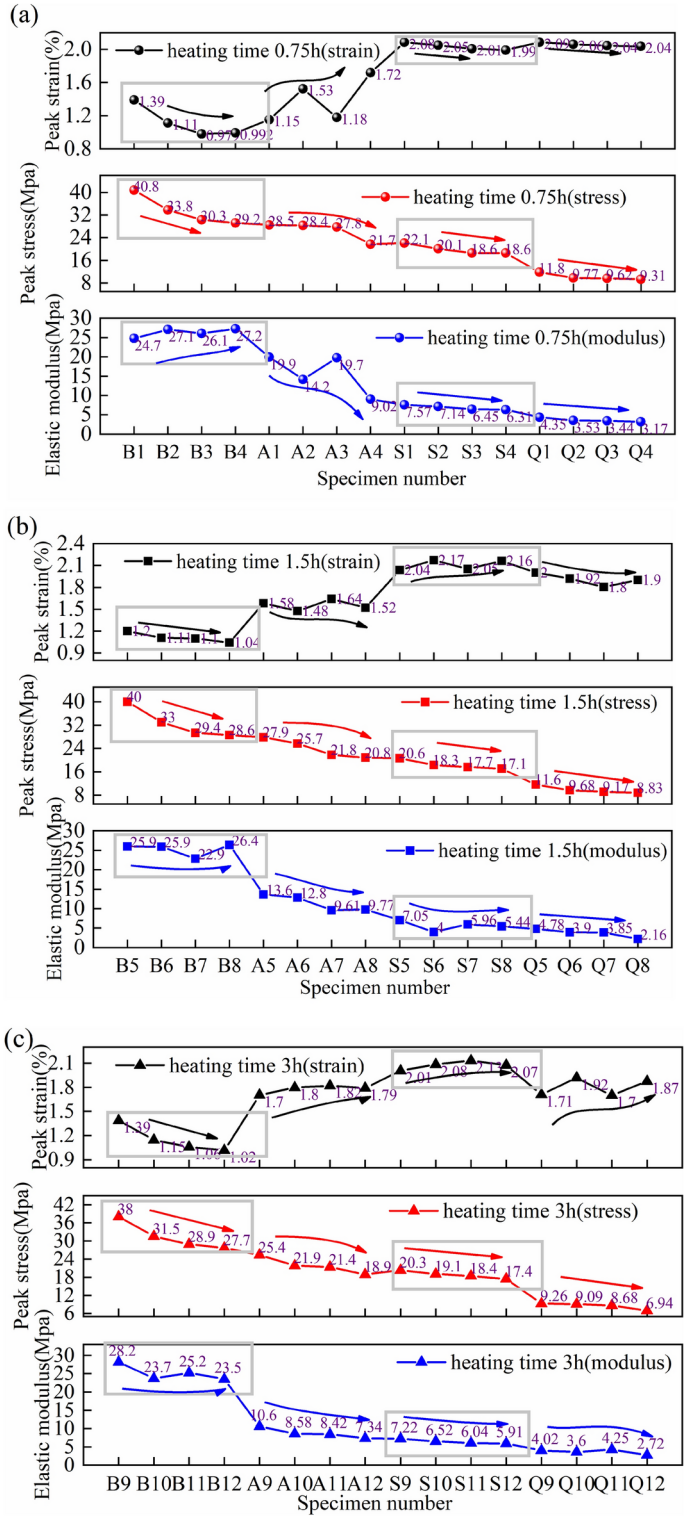

Fig. 6. Change plot of temperature-cooling time.

temperatures reach 1000 °C, although this trend persists, the changes become less pronounced. This shift may be associated with the complete reaction of reactants, the molten structural state, and a fundamental change in the material's nature.

In terms of mechanical properties, the elastic modulus, peak stress, and peak strain are all affected by the temperature, heating time, and cooling time. Specifically, the peak stress is significantly affected by these parameters. Table 4 illustrates the temperature of the specimens post-heating. Analysis reveals that when the cooling time is 0.5 h, the specimens do not fully cool and retain a certain temperature (refer to Table 4). Figures 6

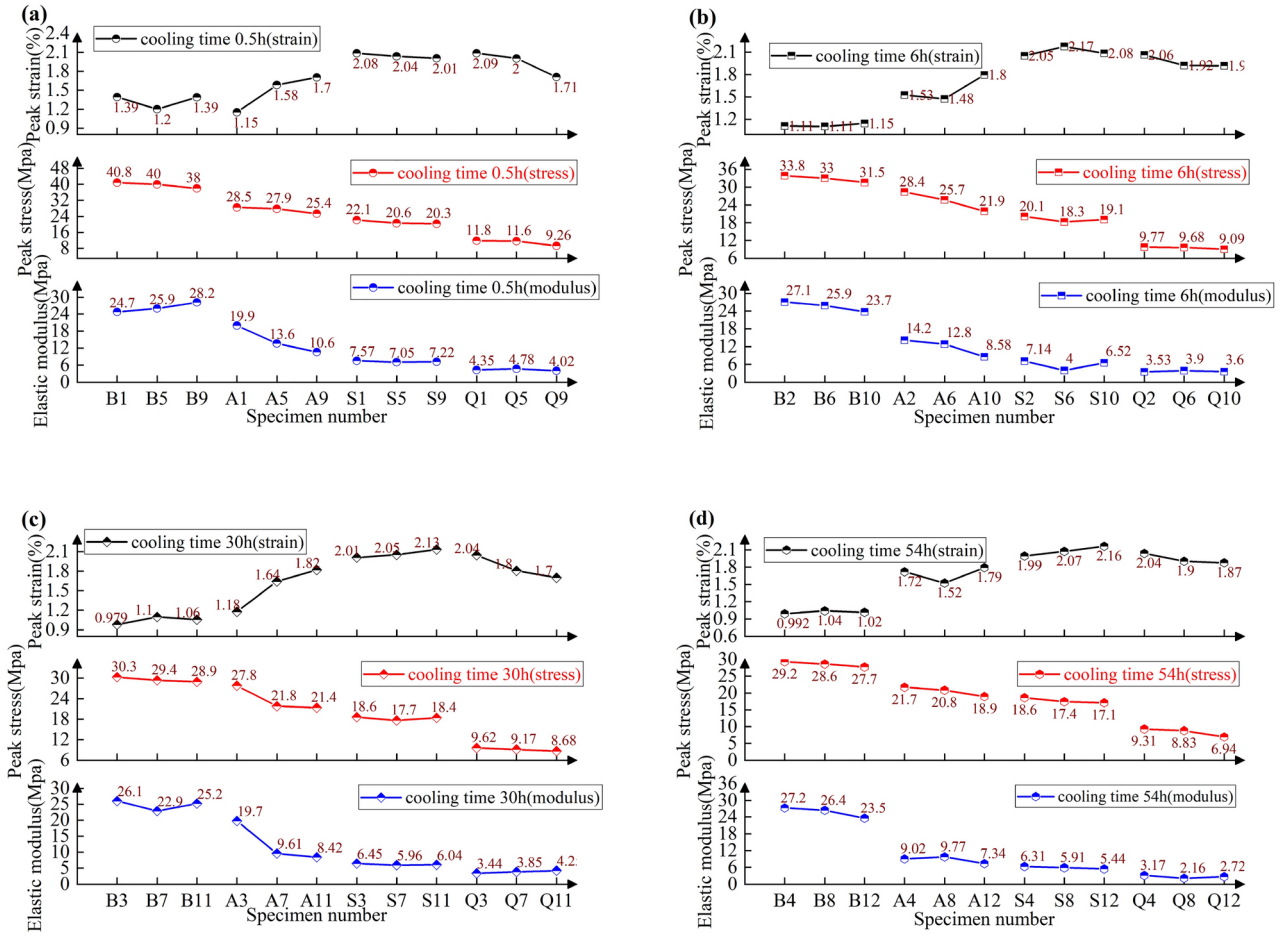

Fig. 7. Temperature-heating time change plot.

Test specimen	Temperature/℃	Test specimen	Temperature/℃	Test specimen	Temperature/℃	Test specimen	Temperature/℃
S0.75–0.5	160.4	A0.75–0.5	110.4	B0.75–0.5	48.2	Q0.75–0.5	162.3
S0.75–6	25	A0.75–6	25	B0.75–6	25	Q0.75–6	25
S0.75–30	25	A0.75–30	25	B0.75–30	25	Q0.75–30	25
S0.75–54	25	A0.75–54	25	B0.75–54	25	Q0.75–54	25
S1.5–0.5	166.8	A1.5–0.5	116.2	B1.5–0.5	63.8	Q1.5–0.5	174.6
S1.5–6	25	A1.5–6	25	B1.5–6	25	Q1.5–6	25
S1.5–30	25	A1.5–30	25	B1.5–30	25	Q1.5–30	25
S1.5–54	25	A1.5–54	25	B1.5–54	25	Q1.5–54	25
S3-0.5	174.2	A3-0.5	118	B3-0.5	73	Q3-0.5	189
S3-6	25	A3-6	25	B3-6	25	Q3-6	25
S3-30	25	A3-30	25	B3-30	25	Q3-30	25
S3-54	25	A3-54	25	B3-54	25	Q3-54	25

Table 4. Temperature change of test specimens after cooling.

and 7 demonstrate that specimens with residual heat exhibit higher peak stresses and elastic moduli at various temperatures and heating durations compared to those that have been fully cooled to room temperature. This phenomenon may be attributed to the presence of internal thermal stresses. Furthermore, increased high temperatures and prolonged heating durations lead to the formation of large pores, holes, intermittent cracks, and dissolved adhesion, which directly impact the peak stress and elastic modulus, resulting in their reduction, while the peak strain correspondingly increases. Additionally, temperature-induced structural changes also affect the elastic modulus of the specimens. Higher temperatures result in a decrease in the feldspar phase, suggesting that extensive feldspar decomposition corresponds to the gradual disappearance of a broad range of pores and honeycomb structures, which transform into a flocculent morphology. Regarding cooling time, stress

reduction is typically associated with a looser internal structure, and the degree of loosening is proportional to the extended cooling period. Longer cooling times lead to more severe weathering of the specimens, increased water absorption, and softer consistency. Interestingly, when the temperature reaches 1000 °C, the impact of cooling time and heating duration on the mechanical properties diminishes, which may be related to the completion of chemical reactions reaching a critical state.

Temperature-force damage constitutive equation

As understanding of the mechanical properties of various rock samples at different temperatures deepens, the development and establishment of a damage constitutive model under multiple factors has increasingly become a crucial benchmark for assessing the degree of damage in rock engineering[32]. Theories such as the Lemaitre strain equivalence hypothesis and the Weibull distribution have established themselves as significant theoretical foundations. Drawing on the Lemaitre strain equivalence hypothesis, Li et al., by the evolution law of internal damage during the stress process of damage mechanics, define the damage threshold as the stress level at which a material begins to exhibit damage. The initial elasticity of rock loading continues after yielding until the stress–strain curve demonstrates residual strength. Additionally, multiple factors are incorporated into the Weibull distribution, leading to the proposal of a new constitutive damage model. This model accurately describes the deformation properties of both residual strength and elastic deformation under low constraint pressure[33]. In their examination of the constitutive model of rock statistical damage, Jiang and researchers developed a model for rock statistical damage post- high-temperature exposure. They employed the M-C criterion, which incorporates thermal damage variables and the Weibull distribution function, to determine the parametric expression[34]. Zhu et al. introduced a thermal damage variable, DT, based on Lemaitre's work, to establish a rock-constitutive model following heat treatment[35], utilizing the Weibull distribution theory. Similarly, Yang et al. proposed a constitutive model that considers both loading rate and temperature, based on the Weibull distribution, to assess the[36] shale damage specimens.

This study evaluates the extent and degree of fire-induced damage to buildings, encompassing both structural and non-structural components. The damage evolution equation, constructed using Weibull intensity distribution, provides a comprehensive explanation of the entire crack extension process. This research introduces cooling time and heating time damage factors, an enhancement over previous studies. These additions contribute to the building temperature-force damage constitutive equation, which is used to measure sandstone damage, thereby improving the characterization and prediction of damage principles under actual conditions. By the Lemaitre strain equivalence hypothesis, strain is chosen as the Weibull distribution variable. Consequently, the resulting damage constitutive model is presented in Eq. (8):

$$\sigma = E_r \varepsilon \exp\left[-\left(\frac{\varepsilon}{F_0}\right)^m\right] \tag{8}$$

Among, E_r is the elastic modulus of the specimen after damage.

The boundary conditions according to the stress–strain test curve are:

$$\begin{cases} \sigma|_{\varepsilon=0} = 0 \\ \dfrac{d\sigma}{d\varepsilon}|_{\varepsilon=0} = E \end{cases} \quad \begin{cases} \sigma|_{\varepsilon=\varepsilon_{\max}} = \sigma_{\max} \\ \dfrac{d\sigma}{d\varepsilon}|_{\varepsilon=\varepsilon_{\max}} = 0 \end{cases} \tag{9}$$

Among, $\sigma_{\max}$ is peak stress;$\varepsilon_{\max}$ is peak strain.

Upon substituting Eq. (9) into the damage constitutive model, the distribution parameters are derived as follows:

$$F_0 = \frac{\varepsilon_{\max}}{\left(\frac{1}{m}\right)^{\frac{1}{m}}} \tag{10}$$

$$m = \frac{1}{\ln \frac{E_r \varepsilon_{\max}}{\sigma_{\max}}} \tag{11}$$

The damage evolution equation and the damage constitutive model are obtained:

$$D = 1 - \exp\left[\ln \frac{\sigma_{\max}}{E_r \varepsilon_{\max}} \cdot \left(\frac{\varepsilon}{\varepsilon_{\max}}\right)^{\frac{1}{\ln \frac{E_r \varepsilon_{\max}}{\sigma_{\max}}}}\right] \tag{12}$$

$$\sigma = E_r \varepsilon \exp\left[\ln \frac{\sigma_{\max}}{E_r \varepsilon_{\max}} \cdot \left(\frac{\varepsilon}{\varepsilon_{\max}}\right)^{\frac{1}{\ln \frac{E_r \varepsilon_{\max}}{\sigma_{\max}}}}\right] \tag{13}$$

In many instances, the accumulation of damage in a rock can be approximated as linear, allowing for the straightforward calculation of damage by summing the effects of each loading event. However, in real-world scenarios, damage accumulation frequently exhibits significant nonlinearity. This is because new damages can alter the stress–strain relationship within the rock, subsequently influencing the progression of damage under future loadings. Consequently, this paper addresses the synchronous damage caused by both heating duration and elevated temperatures. In engineering contexts, this synchronous damage is typically characterized by the

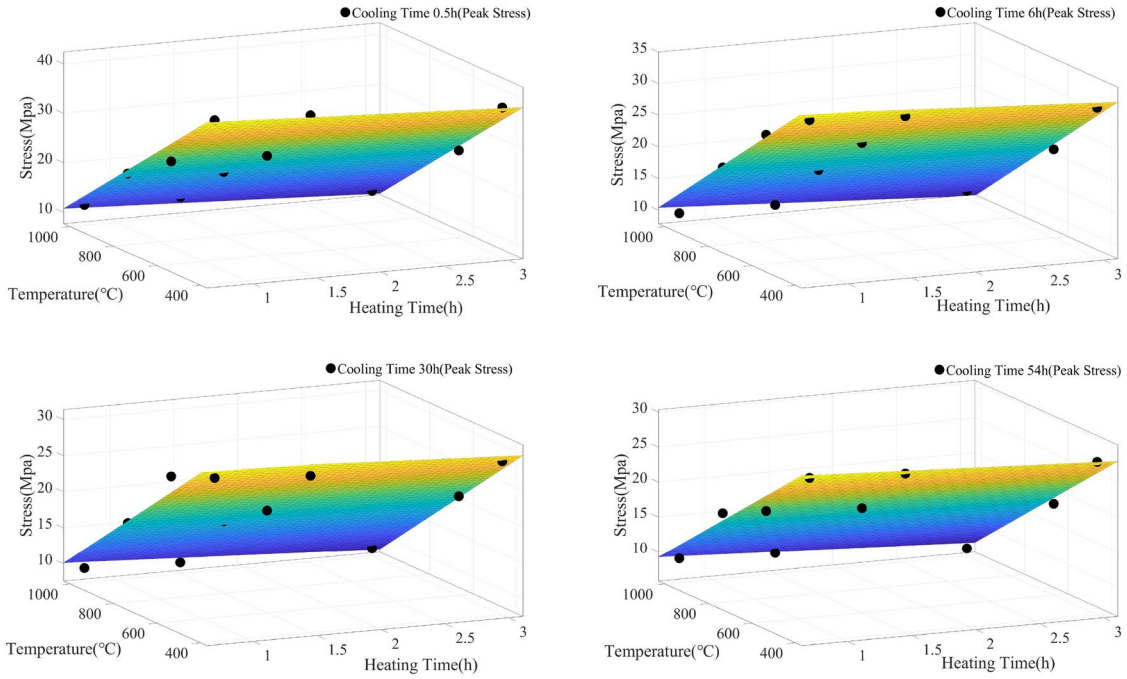

(a)

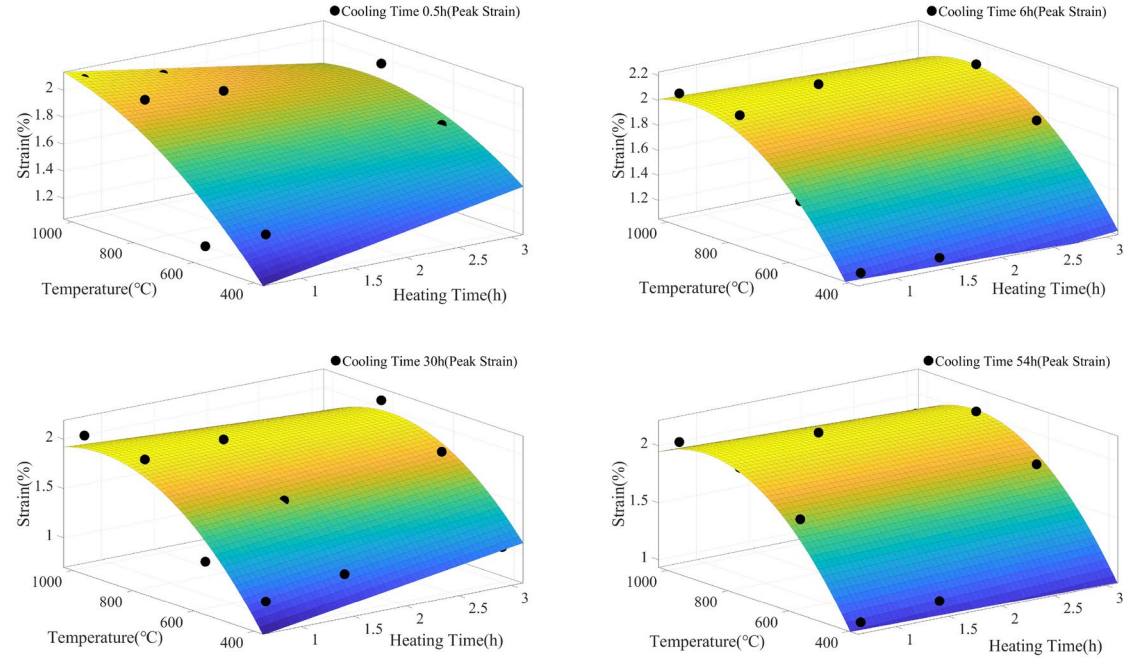

(b)

Fig. 8. Plot of the mechanical parameters and heat exposure for the matlab fits, (**a**) Fitting curve of thermal exposure and peak stress, (**b**) Fitting curve of heat exposure and elastic modulus, (**c**) Fitted curve of thermal exposure and peak strain.

thermal exposure state, defined as the continuous heating of a specimen at a specific temperature for a given duration. This is commonly denoted by the product of temperature (℃) and hours (h). Therefore, the initial phase of the study requires the identification of peak stress; this is followed by an examination of the peak strain and the elastic modulus of the test piece post-damage. The relationship between heating duration and high

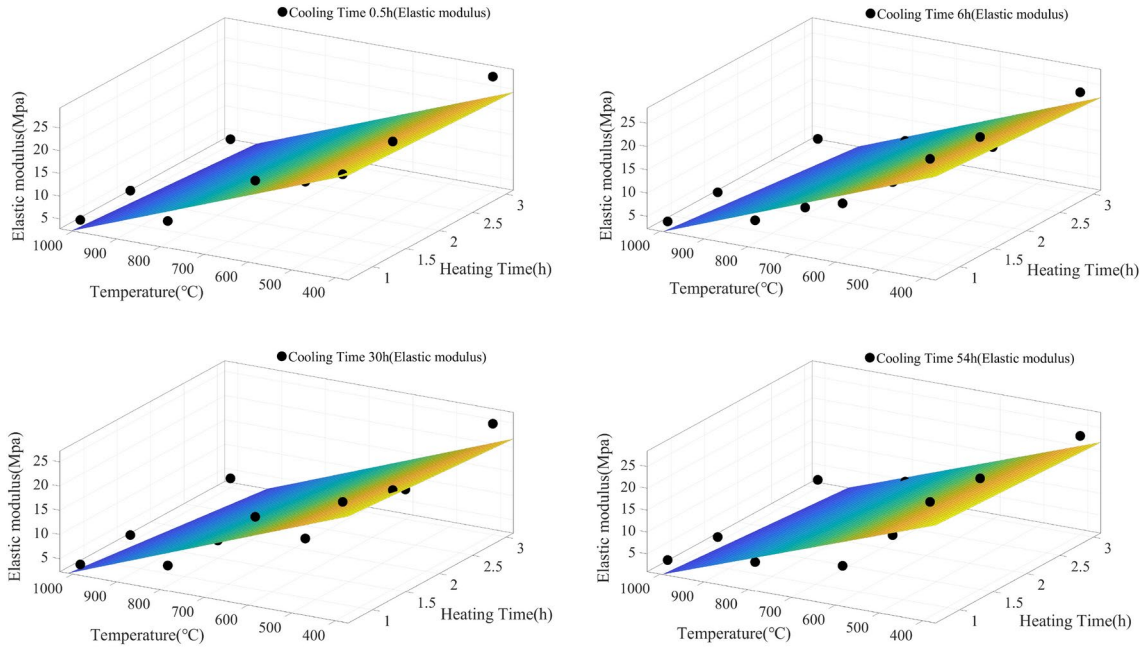

(c)

Figure 8. (continued)

Type	Cooling time	Fitting parameters					Fitting coefficient	Fitting relations
σ_{max} Peak Stress	tc	k_1	k_2	k_3	-	–	R^2	$\sigma_{max} = k_1 * t_h + k_2 * T + k_3$
	0.5	-1.158	-0.0462	59.07	-	–	0.9843	
	6	-1.119	-0.03796	50.22	-	–	0.9779	
	30	-0.8703	-0.03328	44.96	-	–	0.9574	
	54	-0.8523	-0.03163	42.4	-	–	0.9620	
ε_{max} Peak Strain		η_1	η_2	η_3	η_4	η_5	R^2	$\varepsilon_{max} = \eta_1 * t_h + \eta_2 * T + \eta_3 * t_h * T + \eta_4 * T^2 + \eta_5$
	0.5	0.2959	0.004192	-0.0004105	-1.631e-06	-0.3734	0.7338	
	6	0.1463	0.007183	-0.0001737	-3.829e-06	-1.306	0.9302	
	30	0.2976	0.008347	-0.0003538	-4.473e-06	-1.889	0.8591	
	54	0.09062	0.008778	-0.0001233	-4.987e-06	-1.782	0.9647	
E_rElastic modulus		α_1	α_2	α_3	–	–	R^2	$E_r = \alpha_1 * t_h + \alpha_2 * T + \alpha_3$
	0.5	-0.6627	-0.03657	39.92	–	–	0.8865	
	6	-1.002	-0.03581	38.56	–	–	0.8674	
	30	-1.079	-0.03453	37.89	–	–	0.8348	
	54	-0.6948	-0.03596	37.13	–	–	0.8118	

Table 5. Fitting results of heating time and temperature and mechanical parameters.

temperature is then determined and fitted using Matlab. The specific fitted images are presented in Fig. 8, with the numerical results detailed in Table 5.

The aforementioned fitting of peak stress, peak strain, elastic modulus, and heat exposure (comprising high temperature and heating time) was conducted to investigate the damage to the sandstone equivalent model caused by cooling time, heating time, and high temperature. This damage is considered to be nonlinear. The varying cooling times and their corresponding fitting parameters, along with the associated mechanical relationships, were incorporated into the Weibull model. This allowed for an assessment of the damage resulting from the interaction of these three factors. Figure 9 illustrates the secondary fitting relationship and the effect of using cooling time in the fitting process.

Modeling verification

In this study, we fit the new model and introduce boundary conditions to derive it. Compared with the previous model, it can be measured by two factors, the peak stress and the peak strain, which is an optimization

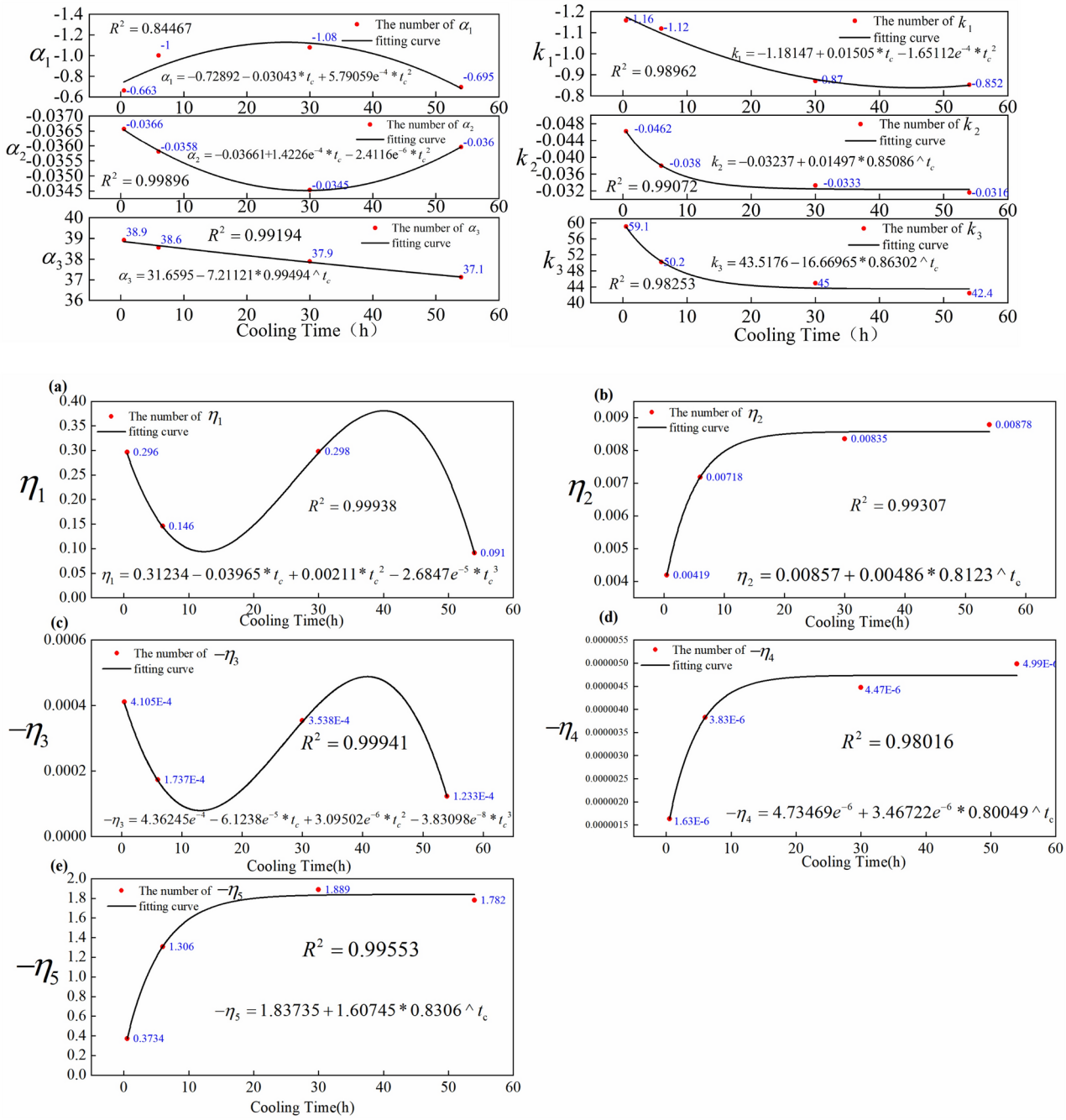

Fig. 9. Secondary fitting relationship and fitting effect after adding cooling factors.

improvement for the model itself. On the other hand, by adding the heating time, cooling time, temperature, peak stress, and peak strain as indicators, a new fitting equation, a secondary improved model, can directly deduce the three factors of the peak strain and the peak stress, considering the previous factors for fitting effect validation using test orthogonal test (Orthogonal Array Testing Strategy, OATS) to peak stress measure specific results as shown in Fig. 10 and Table 6:

Through the orthogonal test verification, the error relative to the model value and the test value is below 5%, and the obtained results can be verified.

Conclusion

This study investigates the damage mechanisms in sandstone affected by heating duration, temperature, and cooling period. The temperature was set at 200 to 800° C, with a cooling time between 0.5 h and 54 h and a heating time between 0.75 h and 3 h. Microscopic analysis using XRD and SEM, along with macroscopic evaluation of mechanical and physical properties, reveals the effects of these variables. A constitutive model is developed to encapsulate the multi-factor damage. Experiments confirm the pivotal role of cooling period,

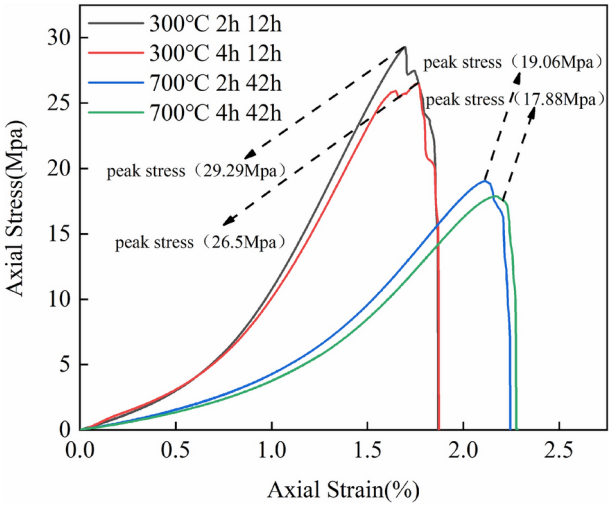

Fig. 10. Verification test stress and strain curve diagram.

temperature	heating time	cooling time	Results of the peak stress model calculation	Results of the peak-strain experiment	fractional error
300℃	2 h	12 h	29.56	29.29	0.9%
300℃	4 h	12 h	27.51	26.5	4.2%
700℃	2 h	42 h	19.15	19.06	0.5%
700℃	4 h	42 h	17.47	17.88	2.3%

Table 6. Comparison of model and validation test data.

heating duration, and temperature on red sandstone damage, supporting the study's design. The findings are summarized as follows:

Microscopic analysis at room temperature identified a massive, honeycomb-like structure in red sandstone specimens, with initial surface cracks due to physical damage. The rock composition includes silica and K/Na/Ca feldspars. Heating induced fine and through-cracks, void formation, and the degradation of the honeycomb structure, culminating in large through-cracks or a liquid-solidification state. Chemical reactions led to the dissolution of feldspar structures. Furthermore, at a constant temperature, extending the heating duration resulted in compositional changes in the sandstone, specifically the disappearance of certain feldspar structures and the emergence of aluminum silicates.

Elevated temperatures induce alterations in the physical characteristics of sandstone, including mass reduction, volumetric expansion, and diminished density. Extended durations of heating and cooling cycles result in physical parameter degradation patterns that mirror the temperature fluctuations. Macroscopic and microscopic analyses encompass the evaporation of water and chemical ionization processes during the heating phase, as well as the weathering and the loosening of the internal structure upon cooling.

Temperature, heating duration, and cooling time are critical factors affecting rock mechanics, with peak stress ranging from 6.94 MPa to 40 MPa under heating (400–1000 °C, 0.75–3 h) and cooling (0.5–54 h) conditions. Short cooling intervals (0.5 h) result in residual heat, leading to increased peak stress due to thermal stress effects. Extended cooling enhances rock fragmentation and damage, decreasing peak stress and increasing peak strain. Higher temperatures and longer heating times promote pore formation, voids, cracking, and adhesion loss, thereby degrading rock structure and modulating peak stress and elastic modulus, with a concomitant rise in peak strain.

This study employed peak stress, peak strain, and elastic modulus from uniaxial compression as baseline data. The Lemaitre strain equivalence hypothesis and Weibull distribution were applied to enhance model boundary conditions. Thermal exposure was integrated, and a peak stress-peak strain relationship was developed via MATLAB. To address the nonlinear damage in rocks, the fitting function coefficient was modified according to cooling time, creating a comprehensive constitutive model. Cross-testing confirmed a model accuracy within 5% of actual values.

This study on rock cooling and continuous heating durations also provides innovative insights into energy sector progress. Future research can utilize various experimental tools (e.g., thermocouples, infrared thermometers, laser thermal imaging) to accurately measure rock temperature changes, enhancing understanding of associated physical and chemical alterations. This work addresses key theoretical challenges in the domain[37].

Data availability

Te datasets generated and analyzed during the current study are not publicly available as the datasets are from the team and are only available for this study, but datasets are available from the corresponding author on reasonable request.

Received: 14 November 2024; Accepted: 23 January 2025
Published online: 31 January 2025

References

1. Tang, F., Wang, L., Lu, Y., & Yang, X. Thermophysical properties of coal measure strata under high temperature. Environmental Earth Sciences, https://doi.org/10.1007/s12665-015-4364-0. (2015).
2. Chen, Z. L., Chen, J. Y., Liu, H. & Zhang, Z. F. Present status and development trends of underground space in Chinese cities: Evaluation and analysis. *Tunnell. Underground Space Technol.* https://doi.org/10.1016/j.tust.2017.08.027 (2018).
3. Momin, M. A., Ahmed, K. S., Mustafy, T. & Islam, M. J. Damage assessment and test results of construction materials of a fire-damaged RC building. *Results Eng.* https://doi.org/10.1016/j.rineng.2024.102986 (2024).
4. Gao, Y. et al. Recognition of rock materials after high-temperature deterioration based on SEM images via deep learning. *J. Mater. Res. Technol.* https://doi.org/10.1016/j.jmrt.2023.05.271 (2023).
5. Hu, X. et al. A micromechanical-based failure criterion for rocks after high-temperature treatment. *Eng. Fracture Mech.* https://doi.org/10.1016/j.engfracmech.2023.109275 (2023).
6. Verma, I. A. K., Jha, M. K., Maheshwar, S., Singh, T. N. & Bajpai, R. K. Temperature-dependent thermophysical properties of Ganurgarh shales from Bhander group. *Environ. Earth Sci.* **75**, 1–11. https://doi.org/10.1007/s12665-015-4992-4 (2016).
7. Li, S., Lin, H., Cao, R., Wang, Y. & Zhao, Y. Mechanical behavior of rock-like specimen containing hole-joint combined flaw under uniaxial loading: findings from DIC and AE monitoring. *J. Materials Res. Technol.* https://doi.org/10.1016/j.jmrt.2023.08.102 (2023).
8. Shen, M. et al. Micro-damage evolution and macro-mechanical property of preloaded sandstone subjected to high-temperature treatment based on NMR technique. *Const. Build. Mater.* https://doi.org/10.1016/j.conbuildmat.2023.130638 (2023).
9. Peng, L. et al. Analysis of physical and mechanical behaviors and microscopic mineral characteristics of thermally damaged granite. *Sci. Rep.* **14**, 14776. https://doi.org/10.1038/s41598-024-65752-4 (2024).
10. Ding, Q. le, Ju, F., Mao, X. B., Ma, D., Yu, B. Y., & Song, S. B. (2016). Experimental Investigation of the Mechanical Behavior in Unloading Conditions of Sandstone After High-Temperature Treatment. Rock Mechanics and Rock Engineering. https://doi.org/10.1007/s00603-016-0944-x
11. Xiao, W., Yu, G., Li, H., Zhan, W. & Zhang, D. Experimental study on the failure process of sandstone subjected to cyclic loading and unloading after high temperature treatment. *Eng. Geol.* https://doi.org/10.1016/j.enggeo.2021.106305 (2021).
12. Yang, S. Q., Huang, Y. H., Tian, W. L., Yin, P. F., & Jing, H. W. Effect of High Temperature on Deformation Failure Behavior of Granite Specimen Containing a Single Fissure Under Uniaxial Compression. Rock Mechanics and Rock Engineering. https://doi.org/10.1007/s00603-018-1725-5. (2019).
13. Li, S., Huang, Z., Yang, D., Zeng, W., & Zhao, K. Study of the Acoustic Characteristics and Evolution of the Failure Mode of Yellow Sandstone Under Uniaxial Compression. Rock Mechanics and Rock Engineering. https://doi.org/10.1007/s00603-023-03637-0. (2024).
14. Yavuz, H., Demirdag, S., & Caran, S. Thermal effect on the physical properties of carbonate rocks. International Journal of Rock Mechanics and Mining Sciences. https://doi.org/10.1016/j.ijrmms.2009.09.014. (2010).
15. Chen, Y. L., Ni, J., Shao, W. & Azzam, R. Experimental study on the influence of temperature on the mechanical properties of granite under uni-axial compression and fatigue loading. *Int. J. Rock Mech. Min. Sci.* https://doi.org/10.1016/j.ijrmms.2012.07.026 (2012).
16. Brotóns, V., Tomás, R., Ivorra, S., & Alarcón, J. C. (2013). Temperature influence on the physical and mechanical properties of a porous rock: San Julian's calcarenite. In Engineering Geology (Vol. 167). https://doi.org/10.1016/j.enggeo.2013.10.012
17. Wu, G., Wang, Y., Swift, G., & Chen, J. (2013). Laboratory Investigation of the Effects of Temperature on the Mechanical Properties of Sandstone. Geotechnical and Geological Engineering. https://doi.org/10.1007/s10706-013-9614-x
18. Yu, J., Chen, S. jie, Chen, X., Zhang, Y. zhou, & Cai, Y. yan. (2015). Experimental investigation on mechanical properties and permeability evolution of red sandstone after heat treatments. Journal of Zhejiang University: Science A. https://doi.org/10.1631/jzus.A1400362
19. Gu, B., Wan, Z., Zhang, Y., Ma, Y. & Xu, X. B. Influence of Real-Time Heating on Mechanical Behaviours of Rocks. *Adv. Civil Eng.* https://doi.org/10.1155/2020/8879922 (2020).
20. Hassani, F., Nekoovaght, P. M., & Gharib, N. (2016). The influence of microwave irradiation on rocks for microwave-assisted underground excavation. Journal of Rock Mechanics and Geotechnical Engineering. https://doi.org/10.1016/j.jrmge.2015.10.004
21. Tang, Z. C., Sun, M. & Peng, J. Influence of high temperature duration on physical, thermal and mechanical properties of a fine-grained marble. *Applied Thermal Engineering* https://doi.org/10.1016/j.applthermaleng.2019.04.039 (2019).
22. Zhang, X. W., Xu, J. H., Cao, Y., Liu, D., Sun, L., & Shaikh, F. On the Microcrack Propagation and Mechanical Behavior of Granite Induced by Thermal Cycling Treatments. Processes. https://doi.org/10.3390/pr10081551. (2022).
23. Kim, K., Kemeny, J., & Nickerson, M. Effect of Rapid Thermal Cooling on Mechanical Rock Properties. Rock Mechanics and Rock Engineering, https://doi.org/10.1007/s00603-013-0523-3. (2024).
24. Wang, H. et al. Investigation of fracture characteristics of cracked granite suffered from different thermal treatments and water-cooling time. *Journal of Materials Research and Technology* https://doi.org/10.1016/j.jmrt.2024.01.060 (2024).
25. Yang, K., Fang, J., Lyu, X., Tang, J., & Liu, W. Uniaxial compression tests on red sandstone specimens after different high temperature processing and cooling time. Bulletin of Engineering Geology and the Environment, https://doi.org/10.1007/s10064-022-02887-6. (2022).
26. Zhang, Z. et al. Performance analysis of an improved temperature control scheme with cold stored in surrounding rock for underground refuge chamber. *Appl. Ther. Eng.* https://doi.org/10.1016/j.applthermaleng.2023.121589 (2024).
27. Mo, C., Zhao, J., & Zhang, D. Real-Time Measurement of Mechanical Behavior of Granite During Heating–Cooling Cycle: A Mineralogical Perspective. Rock Mechanics and Rock Engineering, https://doi.org/10.1007/s00603-022-02867-y. (2022).
28. Chunping, W., Jianfeng, L., Liang, C., Jian, L., Lu, W., & Yilin, L. Creep constitutive model considering nonlinear creep degradation of fractured rock. International Journal of Mining Science and Technology, https://doi.org/10.1016/j.ijmst.2023.11.008, (2024).
29. Experimental study of thermal damage under compression and tension of Makrana marble PK Gautam, MK Jha, AK Verma, TN Singh(2020) Journal of Thermal Analysis and Calorimetry 139, 609–627, https://doi.org/10.1007/s10973-019-08403-5. (2020)
30. Wu, X. H. et al. Research progress on the evolution of physical and mechanical properties of thermally damaged rock. *Gongcheng Kexue Xuebao/Chinese J. Eng.* https://doi.org/10.13374/j.issn2095-9389.2020.12.23.007 (2022).
31. Zhang, Y. & Zhao, G. F. A multiphysics method for long-term deformation analysis of reservoir rock considering thermal damage in deep geothermal engineering. *Renew. Energy* https://doi.org/10.1016/j.renene.2023.01.026 (2023).
32. Chen, Q. et al. Mechanical properties and damage constitutive model of sandstone after acid corrosion and high temperature treatments. *Int. J. Min. Sci. Technol.* https://doi.org/10.1016/j.ijmst.2022.11.011 (2023).

33. Li, H. C. & Zhang, S. A constitutive damage model of rock based on the assumption of modified Lemaitre strain equivalence hypothesis. *Yantu Lixue/Rock and Soil Mech.* https://doi.org/10.16285/j.rsm.2017.05.012 (2017).
34. Zhu, Z. et al. Statistical thermal damage constitutive model of rocks based on Weibull distribution. *Arab. J. Geosci.* https://doi.org/10.1007/s12517-021-06730-2 (2021).
35. Yang, B., Xue, L. & Wang, M. Evolution of the shape parameter in the Weibull distribution for brittle rocks under uniaxial compression. *Arab. J. Geosci.* https://doi.org/10.1007/s12517-018-3689-x (2018).
36. Jiang, H. P., Jiang, A. N. & Yang, X. R. Statistical damage constitutive model of high temperature rock based on Weibull distribution and its verification. *Yantu Lixue/Rock and Soil Mech.* https://doi.org/10.1628/j.rsm.2020.1461 (2021).
37. Verma, A. K., Gautam, P., Singh, T. N. & Bajpai, R. K. Discrete element modelling of conceptual deep geological repository for high-level nuclear waste disposal. *Arab. J. Geosci.* **8**, 8027–8038. https://doi.org/10.1007/s12517-014-1762-7 (2015).

Author contributions

M.Q conducted the experiments and wrote the main manuscript text. Y.S analyzed data and contributed to critical revision of the manuscript. X.W contributed to the design and supervision of experiments. H.N reviewed the pictures in the article and completed the revision. Y.Z analyzed the formal. D.Z performed the article validation test. N.Q conceived the experiments and provided funding. All authors contributed to reviewed the manuscript.

Funding

Liaoning Provincial Key Laboratory of Mine Environment and Disaster Mechanics Open Fund, MEDM2023-B-6, Natural Science Foundation of Shandong Province, ZR2021QE202, Key Laboratory of Ministry of Education on Safe Mining of Deep Metal Mines Open Fund, DM2023Z02.

Declarations

Competing interests

The authors declare no competing interests.

Additional information

Correspondence and requests for materials should be addressed to X.W. or N.Q.